Eur. Phys. J. D (2016) 70: 66
DOI: 10.1140/epjd/e2016-60085-2

THE EUROPEAN PHYSICAL JOURNAL D

Regular Article

Conditions for order and chaos in the dynamics of a trapped Bose-Einstein condensate in coordinate and energy space

Roger R. Sakhel[1,3,a], Asaad R. Sakhel[2,3], Humam B. Ghassib[4], and Antun Balaz[5]

[1] Department of Physics, Faculty of Science, Isra University, 11622 Amman, Jordan
[2] Department of Physics and Basic Sciences, Faculty of Engineering Technology, Al-Balqa Applied University, 11134 Amman, Jordan
[3] The Abdus Salam International Center for Theoretical Physics, Strada Costiera 11, 34151 Trieste, Italy
[4] Department of Physics, University of Jordan, 11942 Amman, Jordan
[5] Scientific Computing Laboratory, Institute of Physics Belgrade, University of Belgrade, Pregrevica 118, 11080 Belgrade, Serbia

Received 9 February 2015 / Received in final form 7 July 2015
Published online 24 March 2016 –

Abstract. We investigate numerically conditions for order and chaos in the dynamics of an interacting Bose-Einstein condensate (BEC) confined by an external trap cut off by a hard-wall box potential. The BEC is stirred by a laser to induce excitations manifesting as irregular spatial and energy oscillations of the trapped cloud. Adding laser stirring to the external trap results in an effective time-varying trapping frequency in connection with the dynamically changing combined external+laser potential trap. The resulting dynamics are analyzed by plotting their trajectories in coordinate phase space and in energy space. The Lyapunov exponents are computed to confirm the existence of chaos in the latter space. Quantum effects and trap anharmonicity are demonstrated to generate chaos in energy space, thus confirming its presence and implicating either quantum effects or trap anharmonicity as its generator. The presence of chaos in energy space does not necessarily translate into chaos in coordinate space. In general, a dynamic trapping frequency is found to promote chaos in a trapped BEC. An apparent means to suppress chaos in a trapped BEC is achieved by increasing the characteristic scale of the external trap with respect to the condensate size.

1 Introduction

Although the literature on chaos is vast [1–24], there is still quite a number of phenomena that need to be explored and understood that would enable full control of chaos. Perhaps a deeper examination of the mechanisms causing chaos is timely. This is necessary, for example, in the construction of quantum computers [17,25–28] because chaos severely reduces the accuracy of a quantum computational process and can even destroy it. The Bose-Einstein condensation (BEC) community is currently interested in eliminating chaos in the dynamics of a BEC to achieve highly accurate quantum computers of the future. There have also been investigations on the chaotic quantum billiard [6,9,29–31], which is a dynamical system deeply related to, and which is used to explain some of the results of, the present study. In general, the present work seeks ways for controlling chaos by obtaining a deeper understanding of the mechanisms that promote it. What is also particular about the present work is that it explicitly examines chaos in energy space. This has rarely been done before to the best of our knowledge.

The chaotic dynamics of a BEC has drawn substantial interest in the last decade or two. Theoretical studies have included chaotic oscillations in an attractive BEC [4], chaos in optical lattices [14,32], the depletion of a BEC in a time-dependent trap [33], the Gross-Pitavskii equation (GPE) with a chaotic potential [34], coherence and instabilitiy in a BEC driven by periodic δ-kicks [35], finite-temperature non-equlibrium dynamics in a BEC [36], as well transitions to instability in a kicked BEC [30,37]. Experimentally, there have been studies of dynamical instabilities of BECs in optical lattices [38,39]. In this paper, we provide a comprehensive investigation of aspects of chaotic dynamics present in a two dimensional GPE.

The goals of the present work are: (1) to obtain conditions for order and chaos in the dynamics of an interacting trapped BEC; and (2) to confirm the existence of chaos in its energy space. Our major task is to understand the origins of chaos in a trapped BEC, particularly when the trapping potential is time-dependent. The existence of chaos is confirmed by well-established methods, such as the phase-space trajectories [4], the energy-space trajectories, and the Lyapunov exponent [1,31].

We consider a trapped BEC excited using a red- or blue-detuned laser potential (RDLP or BDLP, respectively). The dynamic stirring causes the overall trapping

[a] e-mail: rogersakhel@yahoo.com

frequency to vary with time, destroys frequency locking, and thereby causing chaos [10]. In addition, the blue (red)-detuned laser tends to reduce (increase) the phase-space density [40] available for excitations in the combined laser+external potential trap. Indeed, a comparison between the latter effects of different phase-space densities unmasks a considerable difference in the dynamics that is strongly related to the way a laser modifies the energy-level structure of the external trapping potential. This difference enables the effect of phase-space density on the occurrence of chaos to be analyzed. Moreover, the role of quantum effects [16] and trap anharmonicity is particularly revealed in the generation of spatial and energy chaos. Order in the spatial dynamics is then demonstrated not to imply order in the energy dynamics. Moreover, the conclusions reached here discourage in particular the use of an anharmonic trap to surround an optical lattice, e.g., when it comes to the transport of atomic qubits using an optical tweezer to implement collisional quantum gates [27]. This is because the anharmonic trap can cause chaotic oscillations inside the system, which can destroy the process of quantum computation.

Although BECs excited by stirrers have been addressed both experimentally [41–55] and theoretically [27,56–60], using blue [48,50,52,53] as well as red-detuned lasers [40,51,54,61–69], very little attention has been paid to energy dynamics such as the soliton energy [70–72] and the total energy [73]. In addition, a detailed examination of the effects of different phase-space densities (different laser amplitudes) is still lacking. We therefore revisit our previous systems [74,75] with the same excitation methods and analyze their dynamics from a different perspective.

The organization of the paper is as follows. In Section 2, the system of the present study is introduced along with our motivation. Then the GPE with the stirring laser potential is briefly discussed. Next, the physical observables are presented with the Lyapunov exponent acting as an important measure for the degree of chaos. A mode expansion of the GPE wavefunction is also considered from which further information about the chaos in the wavefunction is obtained. In addition, the units and numerics are outlined. In Section 3, the results of the simulations are displayed and discussed. The effect of the phase-space density, trapping frequency, trapping anharmonicity, and quantum effects on chaos are explored in a rigorous manner. In Section 4, the results are analyzed. The irregular dynamics is rigorously tested for order and chaos by well-established methods. In Section 5, the validity of our GPE approach is established. The paper ends with conclusions in Section 6. In Appendix, equations are derived that explain the behavior of the effective trapping frequency of the laser+trap as a function of position and time.

2 Method

The system is a trapped two-dimensional (2D) BEC cut off by a hard-wall box potential (BP) boundary [74,75] and excited by a stirring laser. The external trap varies from harmonic to extremely anharmonic. The split-step Crank-Nicolson (CN) method [76,77] was invoked to solve the 2D time-dependent Gross-Pitaevskii equation (TDGPE) in real time (see Fig. 2 of Ref. [75]). The calculations were conducted using the computing cluster of the Max Planck Institute for Physics of Complex Systems, Dresden, Germany. In essence, this was a heavy computational project where for times of order $t \sim 10^4$ several days of CPU time were required to complete simulations.

2.1 Motivation

The prime motivation in exploring this system is to study chaos in low dimensions. The role played by the hard-wall boundaries is noteworthy as they generate complicated structures in the density patterns of a trapped BEC, including those from the nonlinear Talbot effect [74,78]. These patterns arise from the self-interference of an expanding BEC with reflections coming in from the hard walls. Hard walls are realized experimentally by forming sheets of light [79]. Energy is thereby contained, and can be used to excite the BEC to very high energies. Once excited, it remains in these states for times long enough for chaotic behavior to be explored. Our study has been impelled by a quite relevant investigation by Fujimoto and Tsubota [43] who studied vortex nucleation in a harmonically trapped 2D BEC via an oscillating barrier; however they did not address chaos. Another incentive has been provided from a study of phase effects in a harmonically trapped BEC which is periodically driven to chaotic behavior [80].

The importance of the dimple potential (RDLP) is worth underlining and can be understood from the following points: (1) It increases the phase-space density of the trapped BEC by introducing a richer energy-level structure; (2) it is able to trap and split a fragment from a BEC and to transport it away; and (3) it is experimentally realizable and has been used in quite a number of works. Experimentally, Garrett et al. [40] studied the formation of a BEC in a cigar trap to which a dimple potential was added. Jacob et al. [66] produced in it a BEC of sodium atoms. Theoretically, it has been proposed [57] and used [21,59] to model the kinetics of BEC [81] as well as in an analysis of a BEC in an optical cavity driven by an external beam [10]. The latter work demonstrated that the essential features of the chaotic behavior of a BEC are low-dimensional.

2.2 Gross-Pitaevskii equation and laser potential

The 2D TDGPE, as stated in references [74,75], is

$$\left[-\frac{\partial^2}{\partial x^2}-\frac{\partial^2}{\partial y^2}+\tilde{V}(x,y;t)+\mathcal{G}\left|\varphi(x,y;t)\right|^2-i\frac{\partial}{\partial t}\right]\times\varphi(x,y;t)=0, \quad (1)$$

where

$$\mathcal{G}=\frac{4Na_s}{\ell}\sqrt{2\pi\lambda}, \quad (2)$$

is the coupling constant with N the number of particles, a_s the s-wave scattering length, $\ell = \sqrt{\hbar/m\omega_{ho}}$ a length scale, and $\lambda = \omega_z/\omega_{ho}$ an anisotropy parameter determining the width of the ground-state solution in the z-direction, $\phi_o(z)$ with ω_z the trapping frequency perpendicular to the plane of the BEC. As demonstrated in reference [76], the z-dependence of the 3D TDGPE is integrated out to obtain the 2D form equation (1). $\varphi(x,y;t)$ is the wavefunction of the system, where $\int_{-\infty}^{+\infty} dx \int_{-\infty}^{+\infty} dy|\varphi(x,y;t)|^2 = 1$. As before, $\tilde{V}(x,y;t) = V(x,y;t)/\hbar\omega_{ho}$ is an external potential including the stirring laser and is given by

$$\tilde{V}(x,y;t) = \frac{\sigma}{4}\left(|x|^{p_1} + \kappa|y|^{p_2}\right) + A\exp\{-\beta[x^2 + (y - vt)^2]\}. \quad (3)$$

Here ω_{ho} is the trapping frequency, σ the strength of the external potential with exponents p_1 and p_2, κ the anisotropy parameter, A the amplitude of the stirrer ($A > 0$ for BDLP and $A < 0$ for RDLP), β the exponent determining the width of the stirrer, and v its velocity. In both cases, the stirrer sweeps the BEC starting from the center of the system at time $t = 0$ and moving towards the hard wall in the $+y$-direction. The stirrer exits the BP without returning. $\varphi(x,y;t)$ as well as its gradient $\nabla\varphi(x,y;t)$ are assumed to be zero at the BP-boundary. This is to enforce the hard-wall effect, i.e., imposing a potential of infinite height.

2.3 Energy components and chaos

The total energy is given by [75,82]

$$E(t) = \int d^2\mathbf{r}\left[|\nabla\varphi(x,y;t)|^2 + \tilde{V}(x,y;t)|\varphi(x,y;t)|^2 + \frac{\mathcal{G}}{2}|\varphi(x,y;t)|^4\right], \quad (4)$$

where the limits of the integration are only over the area of the BP. According to reference [83], equation (4) is separated into four terms

$$E(t) = E_{zp}(t) + E_{flow}(t) + E_{osc}(t) + E_{int}(t), \quad (5)$$

keeping in mind that, after the stirrer is removed from the BP, $E(t)$ remains constant while its various contributions still vary with time. Putting the wavefunction in polar form, $\varphi(x,y;t) = \sqrt{\rho(x,y;t)}\exp[i\phi(x,y;t)]$ with $\rho(x,y;t) = |\varphi(x,y;t)|^2$ the density and $\phi(x,y;t)$ the phase, the zero-point kinetic energy becomes

$$E_{zp}(t) = \int d^2\mathbf{r}\left[\nabla\sqrt{\rho(x,y;t)}\right]^2, \quad (6)$$

the kinetic energy of particle flow

$$E_{flow}(t) = \int d^2\mathbf{r}(\nabla\phi)^2\rho(x,y;t), \quad (7)$$

the combined trap potential energy

$$E_{osc}(t) = \int d^2\mathbf{r}\tilde{V}(x,y;t)\rho(x,y;t), \quad (8)$$

and finally the interaction energy

$$E_{int}(t) = \frac{\mathcal{G}}{2}\int d^2\mathbf{r}\rho(x,y;t)^2. \quad (9)$$

Note that the total kinetic energy is given by:

$$E_{kin}(t) = E_{zp}(t) + E_{flow}(t). \quad (10)$$

Comparisons can be made between the dynamics of each of these energy terms for two phase-space densities, obtained by applying two stirring lasers: a barrier with $A > 0$ and a well with $A < 0$. Chaos in energy space manifests itself by any irregular oscillations in the energy components and by plotting the trajectories $(E, \dot{E})$, where E denotes the specific component and $\dot{E} = dE/dt$ the time derivative.

2.4 Radial oscillations and chaos

In coordinate space, the root-mean-square (RMS) radius $R_{rms} = \sqrt{\langle r(t)^2\rangle}$ of the trapped cloud is computed using [75].

$$\sqrt{\langle r(t)^2\rangle} = \left[\int |\varphi(x,y;t)|^2(x^2 + y^2)d^2\mathbf{r}\right]^{1/2}. \quad (11)$$

Chaos is signaled by the irregular oscillatory behavior of R_{rms} and by plotting the trajectories $(X, \dot{X})$ in phase space, where $X = \sqrt{\langle r(t)^2\rangle}$ and $\dot{X} = d\sqrt{\langle r(t)^2\rangle}/dt$.

2.5 Lyapunov exponent

Another very reliable test for chaos is the Lyapunov exponent $\mathcal{L}$ [1,31], which provides a quantitative measure. If after a very long simulation time $\mathcal{L}$ remains positive and almost constant, then this is a strong indication of chaotic dynamics. When $\mathcal{L}$ is zero or negative, then chaos is absent. To calculate $\mathcal{L}$, a nonlinear time-series analysis of the various observables is implemented using the package of Kodba et al. [1]. $\mathcal{L}$ is calculated using the expression [1]

$$\mathcal{L} = \frac{1}{Mt_{evolv}}\sum_{\ell=1}^{M}\ln\left(\frac{L_{evolv}^{(\ell)}}{L_0^{(\ell)}}\right), \quad (12)$$

where L_0 is the Euclidean distance between an initial point $\mathbf{p}(0)$ in the embedding space and its nearest neighbor, τ is the embedding delay, and L_{evolv} is the final distance between them after an evolution for a time-step t_{evolv}. After each t_{evolv}, a replacement step ℓ is attempted in which the code looks for a new nearest neighbor of the evolved initial point. A number M of replacement steps is attempted. The point $\mathbf{p}$ is defined by the vector sequence

$$\mathbf{p}(i) = (x_i, x_{i+\tau}, x_{i+2\tau}, \ldots, x_{i+(m-1)\tau}), \quad (13)$$

obtained from the time series, where m is the embedding dimension and i the time. The variable x stands for any observable.

2.6 Mode expansion

Next, the solution to the TDGPE, $\varphi(x,y;t)$, is expanded into different sets of states: the harmonic oscillator (HO) function $H_n(u)$, the Legendre polynomials $P_n(u)$, and the Cosine function $\cos(n\pi u)$ with $u \in (x,y)$ and $n \in \{n_x, n_y\}$ an integer. For the HO case, the wavefunction becomes the double sum

$$\varphi(x,y;t) = \sum_{n_x=0}\sum_{n_y=0} C_{n_x,n_y}(t) B_{n_x} H_{n_x}(x) B_{n_y} \times H_{n_y}(y) e^{-(x^2+y^2)/2}, \quad (14)$$

n_x and n_y being the HO quantum numbers, $B_n = (n!2^n\sqrt{\pi})^{-1/2}$ the normalization constant of $H_n(x)\exp(-x^2/2)$, and $C_{n_x,n_y}(t)$ are time-dependent mode amplitudes that describe the population dynamics of the states (n_x,n_y). The $C_{n_x,n_y}(t)$ are obtained from equation (14) using the orthogonality of the Hermite polynomials such that

$$C_{n_x,n_y}(t) = \int_{-\infty}^{+\infty} dx \int_{-\infty}^{+\infty} dy \cdot \varphi(x,y;t) \times B_{n_x} H_{n_x}(x) B_{n_y} H_{n_y}(y) e^{-(x^2+y^2)/2}. \quad (15)$$

For $P_n(u)$, one should rescale u by the length of the system L and use $B_n = \sqrt{(2n+1)/2}$ for the normalization constants; similarly for $\cos(n\pi u)$ where $B_n = 1/\sqrt{L}$. In particular, the evolutionary patterns of $C_{n_x,n_y}(t)$ signal chaos or order in the population dynamics of the various basis states after an evaluation of their Lyapunov exponents. In addition, they are an important indicator of allowed and forbidden transitions between the HO states. In passing, it is noted that the expansion (14) is the same as that of the classical field approach [84], except that the mode amplitudes are extracted from a numerical solution of the TDGPE at $T = 0$ K.

2.7 Units

The units and numerics are the same as in our previous work [74,75]; they are reviewed here briefly for reference purposes. $\mathcal{G}$, A, v, β, and t, all have the same units as before [74,75]: the lengths and energies are in units of the trap $a_{ho} = \sqrt{\hbar/(2m\omega_{ho})}$ and $\hbar\omega_{ho}$, respectively. A is in units of $\hbar\omega_{ho}$, β in $(a_{ho})^{-2}$, v in a_{ho}, $t = \tau\omega_{ho}$ is unitless, $\mathcal{G}$ is in $(\sqrt{2}a_{ho}^2)^{-1}$, and κ is unitless. The energies equations (5)–(10) are in units of $\hbar\omega_{ho}$.

2.8 Numerics

Throughout, the following parameter settings are used. For the stirrer, we set $v = 2$ and $\beta = 4$, whereas $|A|$ ranges from 0 to 40. For the external trap, we set $\kappa = 1$ such that it is always isotropic. Initially we set $p_1 = p_2 = 2$ for a harmonic trap, but later set $p_1 = p_2 > 2$ to explore the effect of trap anharmonicity. The number of particles for a given $\mathcal{G}$ can be evaluated from equation (2) with the following information. For ^{87}Rb, the scattering length is $a_s = 5.4$ nm and a suitable trapping frequency is $\omega_{ho} = 2\pi \times 25$ Hz [78]. The trap length is then $\ell = 2.16$ μm (ours is $a_{ho} = \ell/\sqrt{2}$). The anisotropy λ used in equation (2) is set to 10 so that the width of the ground state $\phi_o(z)$ becomes extremely small along the z-direction and the system can be considered 2D. For this λ and a value like $\mathcal{G} = 10$ used here, the number of particles is $N \sim 117$ and the BEC is in the weakly interacting regime. The velocity v by which the stirrer is moved can be converted to standard units by $v \to v a_{ho}\omega_{ho}$. Using the previous information, $v = 1$ in trap units is then equal to 2.4×10^{-4} m/s. The BP length is $L = 20$ (a_{ho}) i.e., $-10 \le x \le 10$ and $-10 \le y \le 10$; that is in SI units the density becomes $n \sim N/L^2 = 1.254 \times 10^{11}$ m^{-2} yielding $na_s^2 \sim 10^{-6}$. The dynamics were mostly displayed for times up to $t = 20$ corresponding to 0.127 s, which is within experimental observation times, e.g., of Donley et al. [85]. In calculating Lyapunov exponents, the simulations were conducted for extended periods of $t = 10\,000$ so as to positively confirm the presence of chaos in the observables (Eqs. (6)–(11)). The simulations are initialized using Method (a) in references [74,75]. As before, the results presented are in the transient stage of the simulation, i.e., after, and not including, the initialization process.

3 Results and discussion

3.1 Effect of phase-space density (laser intensities)

Figure 1 demonstrates the dynamics of the energy components and radial size described by equations (6)–(11) under the effect of a BDLP (left column) and an RDLP (right column) for various values of A but fixed interactions $\mathcal{G}$ in a harmonic trap.

3.1.1 Reduced phase-space density (blue-detuned laser)

Stirring using a BDLP reduces the phase space density of the trapped BEC yielding a small irregularity in the dynamics of its energy components and average radial size of its cloud. R_{rms}, E_{kin}, and E_{osc} display ordered, sinusoidal, oscillatory patterns[1], whereas the dynamics of E_{zp}, E_{flow}, and E_{int} are – from an initial shrewd guess – apparently ordered, but not without some noise and irregularities. The oscillations in E_{zp} arise from oscillations in the density $\rho(x,y;t)$, whereas those in E_{flow} from oscillations in $\rho(x,y;t)$ and the phase $\phi(x,y;t)$. In addition, the oscillations in $\rho(x,y;t)$ arise from the center-of-mass oscillations of the trapped BEC cloud and continue with the same pattern even after the BDLP leaves the BP. The reason for this is explained in Section 3.2 below.

[1] Viewed from a spatial point of view then, the GPE is integrable as its behavior is predictable in the latter space.

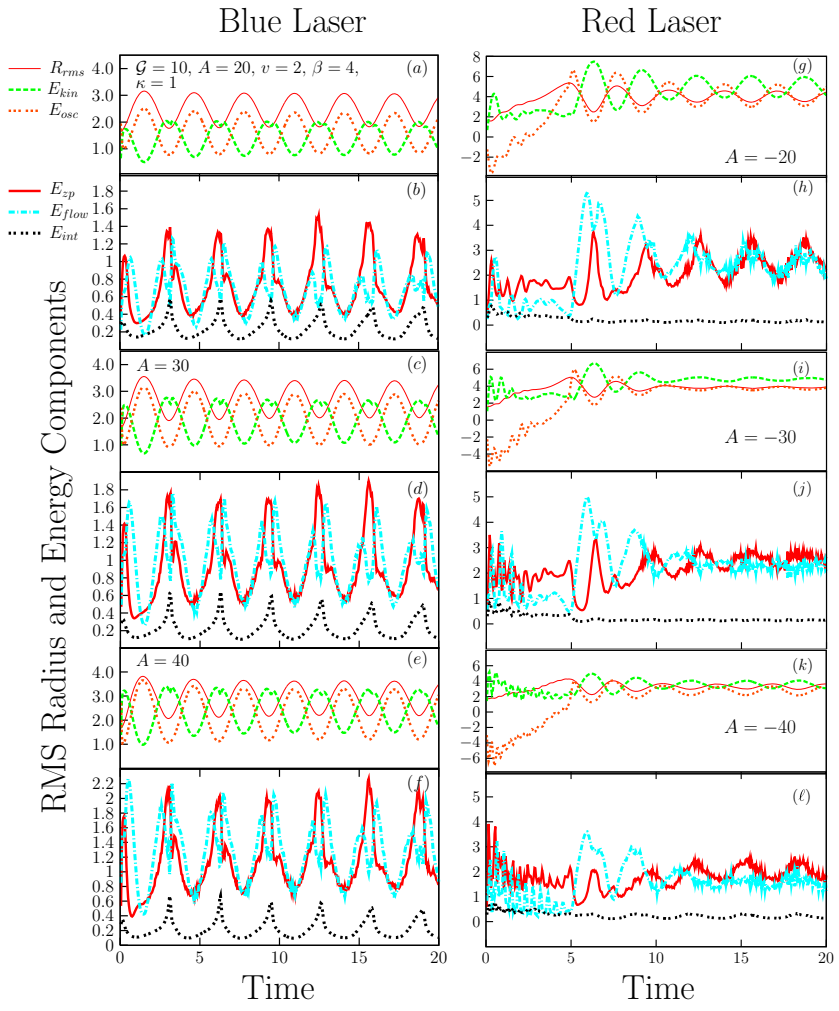

Fig. 1. Spatial and energy dynamics of an interacting Bose gas confined by a two-dimensional harmonic trap cut off by a BP [74,75] and various stirring laser amplitudes A. The side length of the BP is $L = 20$ such that $x \in [-10, 10]$ and $y \in [-10, 10]$. The Bose gas is excited by a stirring blue-detuned laser ($A > 0$ left column) and a red-detuned laser ($A < 0$ right column). The parameters of the system are [74,75]: $\mathcal{G} = 10$, $\beta = 4$, $v = 2$, $p_1 = p_2 = 2$, and $\kappa = 1$. $A = 20$ (frames (a) and (b)), 30 ((c) and (d)), and 40 ((e) and (f)). $A = -20$ ((g) and (h)), -30 ((i) and (j)), and -40 ((k) and (l)). Solid line: R_{rms}; dashed line: E_{kin}; triple-dotted line: E_{osc}; thick solid line: E_{zp}; dashed-dotted line: E_{flow}; double-dotted line: E_{int}. A is in units of $\hbar\omega_{ho}$, β in $(a_{ho})^{-2}$, v in a_{ho}, $\mathcal{G}$ is in $(\sqrt{2}a_{ho}^2)^{-1}$, R_{rms} in a_{ho}, and energy is in $\hbar\omega_{ho}$. κ and $t = \tau\omega_{ho}$ are unitless.

A change in the amplitude of the BDLP yields no qualitative changes in the dynamics. This is because the BDLP introduces only a circular 'hole' in the BEC with no introduction of additional lower energy levels, unlike the RDLP case, which increases the phase-space density. In essence, the effect of a blue-detuned laser is similar to a hard-disk-like obstacle which moves through a 2D fluid.

3.1.2 Enlarged phase-space density (red-detuned laser)

RDLP stirring introduces a larger phase-space density that leads to higher degrees of irregular behavior and causes a strong time-dependent asymmetry of $|\varphi(x, y; t)|^2$ about the x-axis. This yields irregular interference patterns that translate to chaotic behavior. In comparison, the BDLP results in a much weaker asymmetry of $|\varphi(x, y; t)|^2$. Now, although the excitations induced by the RDLP cause somewhat regular oscillations in R_{rms}, E_{kin}, E_{osc}, and E_{int}, the other quantities like E_{zp} and E_{flow} reveal irregular oscillations throughout. For E_{zp} and E_{flow} this can be understood based on them being connected to gradients $\nabla|\varphi(x, y; t)|$ and $\nabla\phi(x, y; t)$, respectively, as they strongly change with time and with a high degree of randomness.

The BEC fragment trapped inside the RDLP undergoes density oscillations at a frequency equivalent to the effective trapping frequency, ω_q, of the combined trap that in turn yields oscillations in $\rho(x, y; t)$ as well. According to equation (A.7), ω_q rises with "increasing" depth $A < 0$ and because E_{zp} and E_{flow} are connected to the $\rho(x, y; t)$ via equations (6) and (7), their oscillation frequency at $t < 5$ rises significantly. These oscillations are not observed in the BDLP case because ω_q remains roughly equivalent to that of the external trap and is smaller than that for the

RDLP case. Also, the availability of energy levels and the dynamic ω_q can be argued to induce irregular oscillatory patterns because of the absence of frequency locking [10][2]. Note that the influence of these initial strong excitations via the red-detuned laser remains even after it has left the trap, as can be seen by the irregular dynamics of E_{zp} and E_{flow} at $t > 5$. The conclusion is that once chaos has been established, it is irreversible.

3.2 Effective trapping frequency

Earlier it was argued that irregularity (chaos according to Ref. [16]) is induced by quantum effects arising from the zero-point motion. The latter is controlled by ω_q and because a time-dependent trapping potential yields a dynamic ω_q (Appendix A) examining its role in irregular behavior as governed by different phase-space densities is therefore important. Now, $\tilde{V}(x, y; t)$ (Eq. (3)) has an effective ω_q defined as:

$$\omega_q(x, y; t) = \sqrt{\frac{\partial^2 \tilde{V}(x, y; t)}{\partial q^2}}, \tag{16}$$

close to the minimum of $\tilde{V}(x, y; t)$ where $q \equiv x, y,$ or z. That is, ω_q can vary spatially as well. It is however expected that $\tilde{V}(x, y; t)$ influences the patterns of the induced irregularities only when ω_q changes with time. Indeed, equation (16) is only applicable to the red-detuned laser with $A < 0$ and it cannot be applied to the blue-detuned laser with $A > 0$, except when the BDLP is exactly centered at the origin of the external harmonic trap. At this point only, the BDLP is surrounded by a circular trough containing a circle of the potential minima loci. In that sense, the BDLP is only an obstacle and it turns out that its motion inside the BEC yields absolutely little change in ω_q in contrast to the RDLP. We provide further support for this conjecture in the following argument. In Figure 1, the blue laser induces oscillations in the dynamics which have almost the same pattern and frequency before and after the laser leaves the BP, whereas they are largely different for the red-detuned laser. One origin of this difference is that the blue-detuned laser does not trap any bosons unlike the red-detuned laser, and consequently the removal of the BDLP from the trap does not affect ω_q. Therefore, the frequency of oscillations remain by and large controlled by the external harmonic trap. In contrast, the RDLP conveys a larger effective trapping frequency to the whole system. When the red-detuned laser leaves the trap, ω_q changes back to that of a pure harmonic oscillator. As a result, the dynamics display different behavior before and after the removal of the RDLP.

[2] Indeed, in reference [10] it was argued that the appearance and disappearance of chaos is due to the transition from quasiperiodic behavior to frequency locking and vice versa. When the RDLP leaves the box potential at $t > 5$, the oscillations of E_{zp} and E_{flow} remain irregular since the BEC is in a highly excited state and frequency locking is absent.

3.3 Effect of trap anharmonicity

We now turn to anharmonic traps. From Figure 2, it is demonstrated that such traps mainly cause irregular oscillations in coordinate and energy space. Both sets of plots demonstrate an apparent increase in irregularity and frequency of the oscillations with increasing $p_1 = p_2$. A similar irregularity was reported earlier by Mateos and José [86] for a particle inside a rigid BP with a periodically oscillating square-potential barrier inside the box. The latter behavior has been identified as chaotic purely from observations of energy oscillations.

An increase in $p_1 = p_2$ yields a larger ω_q (see Eqs. (A.2) and (A.3)), that in turn increases the frequency at which the BEC fragment oscillates inside the RDLP. For example, according to equation (A.13) for $p_1 = p_2 = 7$, ω_q increases with time, and with it the number of HO modes, until the moving RDLP leaves the trap. The stronger anharmonicity generates oscillations in the energy components to become more irregular than in Figure 1 and to 'wash out' the difference between the blue and red-detuned laser. At this point, the BEC is in such a highly excited state with strong irregular dynamic behavior, that the vastly different phase-space densities can no longer be distinguished.

3.4 Quantum effects

In this section, we follow Kapulkin and Pattanayak [16] in an artificial modification of the relative Planck's constant to examine the role of quantum effects in the emergence of chaos or irregularity in the TDGPE. The latter is rescaled in a manner described below so as to introduce this constant via a multiplicative factor Γ into the kinetic energy operator

$$\hat{H}_{kin} = -\Gamma \nabla^2, \tag{17}$$

from which it follows that E_{zp} (Eq. (6)) and E_{flow} (Eq. (7)) become weighted by Γ. One can justify the introduction of Γ in equation (17) based on the following argument. In reference [16], a factor $\beta_0 = \sqrt{\hbar/(m\ell_0^2\omega_{ho})}$ was introduced that identifies a ratio between the characteristic scales associated with a BEC [$\ell = \sqrt{\hbar/(m\omega_{ho})}$] and the trap ($\ell_0$). Let us define $\ell_0 = \sqrt{\hbar/(m\omega_0)}$, which can be different from ℓ. Further, let us introduce an artificial Planck's constant $\hbar_0$ so that $\ell_0 = \sqrt{\hbar/(m\omega_0)} \equiv \sqrt{\hbar_0/(m\omega_{ho})}$ and therefore

$$\sqrt{\Gamma} = \hbar/\hbar_0 = \omega_0/\omega_{ho} = (\ell/\ell_0)^2. \tag{18}$$

That is, a change of the relative Planck's constant $\sqrt{\Gamma}$ amounts to a change in the "relative" characteristic scale ℓ/ℓ_0. For brevity, $\Gamma = (\hbar/\hbar_0)^2$ is referred to as the relative constant and one can then consider rescaling the TDGPE

$$\left[-\frac{\hbar^2}{2m}\nabla^2 + V(x, y; t) + g|\varphi|^2\right]\varphi = i\hbar\frac{\partial}{\partial t}\varphi. \tag{19}$$

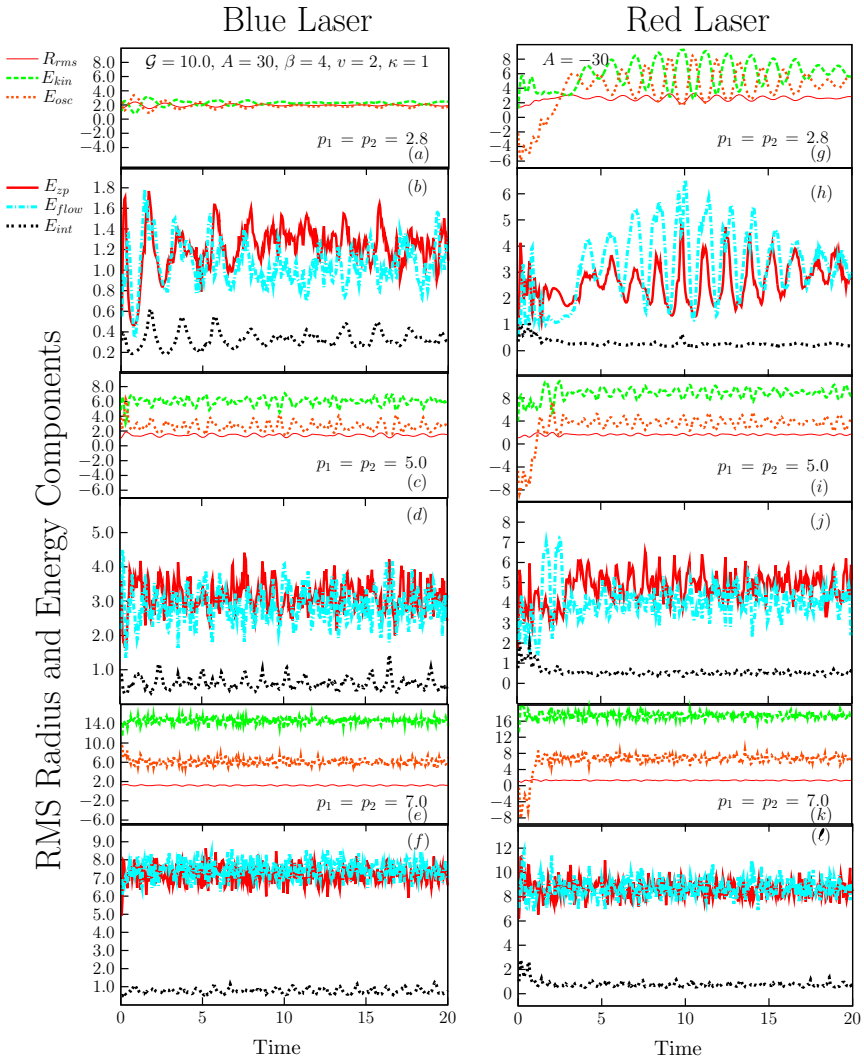

Fig. 2. Same as in Figure 1 with the same labels; but for varying anharmonicities $p_1 = p_2$. The interactions are fixed at $\mathcal{G} = 10$, the stirrer height is $A = 30$ in the left column and its depth is $A = -30$ in the right column. Frames (a), (b), (g), (h): $p_1 = p_2 = 2.8$; (c), (d), (i), (j): 5.0; (e), (f), (k), (l): 7.0. A is in units of $\hbar\omega_{ho}$, $\mathcal{G}$ in $(\sqrt{2}a_{ho}^2)^{-1}$, v in a_{ho}, β in $(a_{ho})^{-2}$, and $t = \tau\omega_{ho}$ and κ are unitless.

by a rescaling of the coordinates x and y in units of $a_{ho} = \ell_0/\sqrt{2}$. That is, one considers $\widetilde{x} = x/a_{ho}$ and $\widetilde{y} = y/a_{ho}$ and divides equation (19) by $\hbar_0\omega_{ho}$ so that it becomes

$$\left[-\Gamma\widetilde{\nabla}^2 + \frac{1}{4}\widetilde{\sigma}\left(|\widetilde{x}|^n + |\widetilde{y}|^n\right) + \widetilde{g}|\varphi|^2\right)\Big]\varphi = i\frac{\partial}{\partial\widetilde{t}}\varphi, \qquad (20)$$

where $\widetilde{\sigma} = \sigma a_{ho}^n/(\hbar_0\omega_{ho})$, $\widetilde{g} = g/(\hbar_0\omega_{ho})$, and $\widetilde{t} = \omega_{ho}t/\sqrt{\Gamma}$. When Γ is small, the characteristic scale associated with the trapping potential is large with respect to the condensate size. Consequently, as $\Gamma \to 0$ the BEC wavefunction tends to become localized rather like a wave packet representing a classical particle. When Γ is large, the BEC extends over a considerable region and quantum effects become visible.

By artificially increasing Γ to values larger than 1, the frequencies of the spatial and energy oscillations increase and their dynamics become more irregular (Fig. 3). This is consistent with results of Kapulkin and Pattanayak [16].

The question then arises: will chaos vanish if we set Γ below 1? Figure 4 displays the dynamics for a significantly lowered $\Gamma = 0.1$ and it is obvious that the frequency of the oscillations is largely reduced in frames (a) and (b), as compared with that for Figure 3. A significant result then is that the quantum effects are the sole reason for any high-frequency oscillations in the BEC dynamics.

If we examine Figure 4c, then as a result of lowering Γ, the oscillations are seen to reduce substantially in R_{rms}, E_{zp} and E_{int} as compared with those in Figures 2e and 2f, but they nevertheless remain active in E_{osc}, E_{kin} and E_{flow}. The persistence of oscillations in an anharmonic trap in the presence of reduced quantum effects is a manifestation of the role of anharmonicity in inducing this behavior in conjunction with the chaotic billiard effect. In frames (a) and (b), chaos has vanished, demonstrating that the reduction of Γ is one way to suppress chaos.

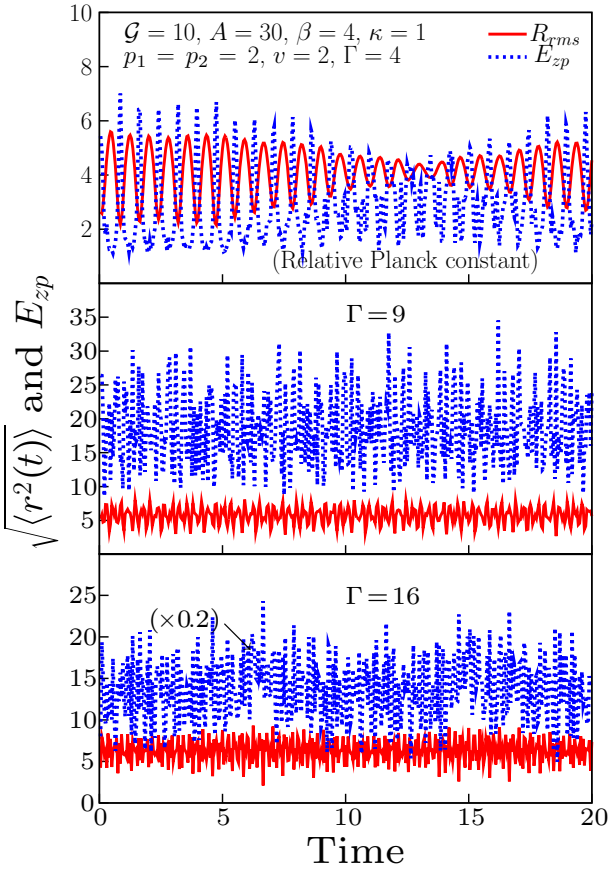

Fig. 3. Quantum effects on the dynamics of a trapped Bose gas. The system is the same as in Figure 1 for $A = +30$; but with increased relative constant Γ. The solid line is $R_{rms}(t) = \sqrt{\langle r^2(t)\rangle}$ and the dashed line $E_{zp}(t)$. Top frame: $\Gamma = 4$; middle frame: 9; and bottom frame: 16. In the bottom frame $E_{zp}(t)$ is reduced by a multiplicative factor of 0.2 to make $R_{rms}(t)$ visible and not to clutter the figure. $R_{rms}(t)$ is in units a_{ho}, $E_{zp}(t)$ in $\hbar\omega_{ho}/\sqrt{\Gamma}$ (see text), A in $\hbar\omega_{ho}/\sqrt{\Gamma}$, $\mathcal{G}$ in $(\sqrt{2}a_{ho}^2)^{-1}$, v in a_{ho}, β in $(a_{ho})^{-2}$, and $t = \tau\omega_{ho}/\sqrt{\Gamma}$ and κ are unitless.

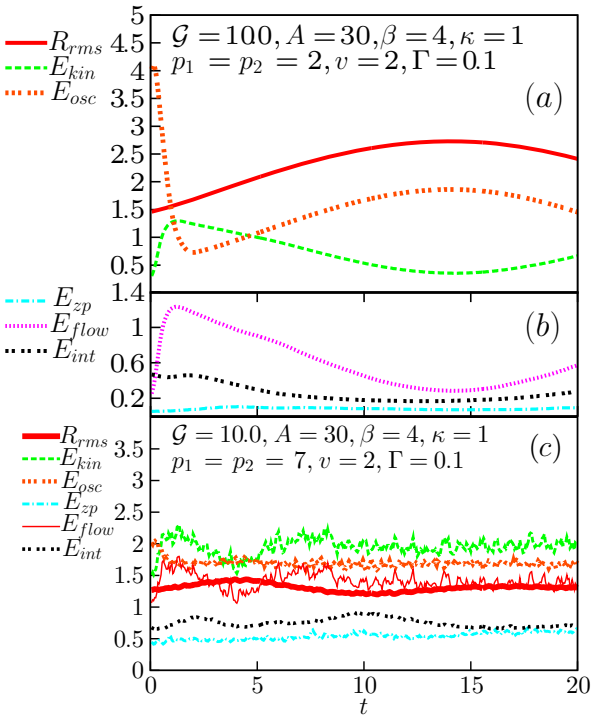

Fig. 4. Frames (a) and (b): Dynamics of the harmonically trapped system in Figure 1 at $A = +30$ for an artificially reduced relative constant $\Gamma = 0.1$. Solid line: $R_{rms}(t)$; dashed line: $E_{kin}(t)$; triple-dotted line: $E_{osc}(t)$; dashed-dotted line: $E_{zp}(t)$; fine-dashed line: $E_{flow}(t)$; double-dotted line: $E_{int}(t)$. Frame (c) is as in frames (a) and (b); but for the anharmonically trapped system in Figures 2e and 2f with $A = +30$. Thick solid line: $R_{rms}(t)$; dashed line: $E_{kin}(t)$; triple-dotted line: $E_{osc}(t)$; dashed-dotted line: $E_{zp}(t)$; thin solid line: $E_{flow}(t)$; and double-dotted line: $E_{int}(t)$. Lengths and energies are in units of the trap a_{ho} and $\hbar\omega_{ho}/\sqrt{\Gamma}$, respectively. A is in units of $\hbar\omega_{ho}/\sqrt{\Gamma}$, $\mathcal{G}$ in $(\sqrt{2}a_{ho}^2)^{-1}$, v in a_{ho}, β in $(a_{ho})^{-2}$, and $t = \tau\omega_{ho}/\sqrt{\Gamma}$ and κ are unitless.

4 Analysis of results

4.1 Physical versus numerical chaos

Brézinova et al. [8] have devised powerful tests for detecting the presence of numerical chaos that could result from the nonintegrability of the TDGPE. Two of these tests are: (1) the conservation of total energy and (2) time-reversal propagation. So far it has already been demonstrated [75] that the total energy of our systems is conserved once the stirrer has left the trapping area. For test (2), a time-reversed evolution of the system has been performed that begins at some chosen time t_0 along the energy dynamics after the stirrer has left the BEC and the energy has stabilized. Let us consider a wavefunction $\psi_{\pm}(\mathbf{r}, t)$, which evolves "forward" $(+)$/"backward" $(-)$ in time. Once $\psi_{+}(\mathbf{r}, t)$ has evolved from a time t to t_0, its propagation is reversed from t_0 to t' (where $t_0 > t'$) according to

$$\psi_{-}(\mathbf{r}, t') = U_{-}(t', t_0)\psi_{+}(\mathbf{r}, t_0), \tag{21}$$

where U_{-} is the propagator that reverses the evolution of $\psi_{+}(\mathbf{r}, t)$. If the forward evolving $\psi_{+}(\mathbf{r}, t)$ equals the backward evolved $\psi_{-}(\mathbf{r}, t')$ at some common time $t = t'$, then numerical chaos is excluded. For a graphical comparison between forward- and reversed-evolving properties, the former are plotted from $t = 0$ to $t = t_0$, and the latter against $t = 2t_0 - t'$ from $t = t_0$ to $t = 2t_0$. That is, $t \in [0, t_0]$ corresponds to increasing time for $\psi_{+}(\mathbf{r}, t)$ and $t \in [t_0, 2t_0]$ corresponds to decreasing times $t' \in [t_0, 0]$ for $\psi_{-}(\mathbf{r}, t')$.

Figure 5 displays this comparison where it can be seen that the dynamics are exactly symmetric about the $t = t_0$ axis. From this, we conclude that any chaos demonstrated in this work is physical and not numerical.

4.2 Chaos and order in the weights of bases states

The goal now is to search for signals of chaos in the GP wavefunction via the mode expansion equation (14). Upon excitation, the trapped Bose gas is energized to a number

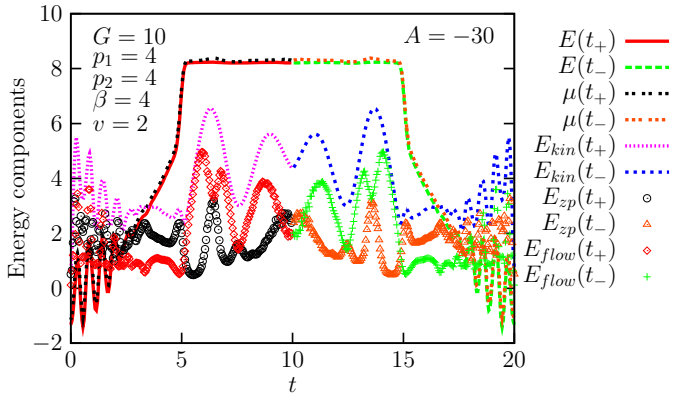

Fig. 5. Checking for the presence of physical or numerical chaos in the Crank-Nicolson code applied in this work. The figure shows forward and backward evolving properties of a trapped BEC excited by an RDLP. The system is the same as in Figure 1 for $A = -30$; except for $p_1 = p_2 = 4$. The $\pm$ subscripts in the labels are for forward/backward evolution in time: Thick solid line: total energy $E(t_+)$; dashed line: $E(t_-)$; double-dotted line: chemical potential $\mu(t_+)$; triple-dotted line $\mu(t_-)$; fine-dotted line: kinetic energy $E_{kin}(t_+)$; dotted line: $E_{kin}(t_-)$; open circles: zero-point energy $E_{zp}(t_+)$; open triangles $E_{zp}(t_-)$; diamonds: kinetic flow energy $E_{flow}(t_+)$; and crosses: $E_{flow}(t_-)$. In this figure, the time at which time reversal begins is $t_0 = 10$ (see text); to the left of t_0, the properties are evolving forward in time t, whereas to the right of t_0, the time axis is for $t = 2t_0 - t'$, where t' is decreasing as the properties are evolving backward in time. Lengths and energies are in units of the trap, a_{ho} and $\hbar\omega_{ho}$, respectively. A is in units of $\hbar\omega_{ho}$, $\mathcal{G}$ in $(\sqrt{2}a_{ho}^2)^{-1}$, v in a_{ho}, β in $(a_{ho})^{-2}$, and $t = \tau\omega_{ho}$ is unitless.

of HO states. The transitions between these states tend to be irregular and it turns out that this is one source of chaos in the wavefunction. It must therefore be emphasized that any chaos appearing in the total wavefunction $\varphi(x, y; t)$ is translated to chaos in the observables under current study (Eqs. (6)–(11)). Within this context, Figure 6 displays the dynamics of $|C_{n_x,n_y}(t)|$. Four cases are considered: two for a BEC in a harmonic trap, which evolve in the presence and absence of a laser, and likewise two for a BEC in an anharmonic trap. From this, the dynamics of $|C_{n_x,n_y}(t)|$ gives a measure for the frequency of particle transitions from one HO state to another and indicates whether one has chaos or order. Frame (I) refers to a BEC in a harmonic trap without a laser. The $|C_{n_x,n_y}(t)|$ with (n_x, n_y) even numbers are almost constant with time and their values range from order $\sim 10^{-2}$ to order 1. This constancy indicates order in $\varphi(x, y; t)$. The largest occupancy is, as expected, for the $(0, 0)$ state and some excitations to higher states with even (n_x, n_y) are due to the initialization of the system in CN simulations [74,75]. $|C_{n_x,n_y}(t)|$ in frame (b) with either n_x or n_y odd are negligible of order $\sim 10^{-9}$ and are rather noisy. These oscillations are however insignificant because their weights are vanishingly small. The difference in weights between frames (a) and (b) is attributed to the following: In the absence of a stirrer, $\varphi(x, y; t)$ is even, i.e., symmetric about the x and y axes. Therefore, only even HO functions [even $H_{n_x}(x)$ and $H_{n_y}(y)$] contribute to the dynamics; the odd functions yield almost zero contribution such that $|C_{n_x,n_y}(t)| \to 0$. Frame (II) refers to a BEC in a harmonic trap with a laser. In this, $|C_{n_x,n_y}(t)|$ reveals nearly periodic oscillations for almost all (n_x, n_y) and range from order 10^{-2} up to 10^{-1}. However, this is not enough to cause ordered oscillations in the right column of Figure 1. Because $\varphi(x, y; t)$ is now antisymmetric about the x-axis, states with odd n_x or n_y display now larger weights than in frame (I,b) when they were practically unoccupied giving only a noisy pattern.

Frame (III) refers to a BEC in an anharmonic trap without a laser. In (a), $|C_{0,0}(t)|$ is almost constant in the absence of a laser. $|C_{2,2}(t)|$ oscillates almost regularly whereas the $|C_{n_x,n_y}(t)|$ for (4,4), (6,6), and (8,8) are now chaotic. Indeed, even if only one state (n_x, n_y) is chaotic, all the dynamical quantities that can be obtained from $\varphi(x, y; t)$ will be chaotic. In frame (b), (5,2), (6,3), and (8,3) show a noisy pattern as in frame (I,b) of negligible amplitude but are not expected to contribute to the overall dynamic behavior of $\varphi(x, y; t)$. Frame (IV) is for a BEC in an anharmonic trap with a laser. In this, some ordered oscillations appear in $|C_{0,0}(t)|$, $|C_{2,2}(t)|$, and $|C_{4,4}(t)|$ whereas $|C_{5,2}(t)|$ seems to be almost zero. The remainder of $|C_{n_x,n_y}(t)|$ are chaotic and their values are largely of order $\sim 10^{-2}$. The latter can be related to the chaos displayed in the right column of Figure 2. Therefore, the anharmonic trap yields irregular oscillations in $|C_{n_x,n_y}(t)|$ that manifest as chaotic oscillations in the physical observables.

4.3 Lyapunov exponents in different bases

The unique signature for chaos in the expansion coefficients $C_{n_x,n_y}(t)$ is again a positive $\mathcal{L}$. Hence, we analyze chaos in the GP wavefunction itself by expanding it in different bases to examine whether chaos in $|C_{n_x,n_y}(t)|$ is basis invariant. Figure 7 displays $\mathcal{L}$ for the $|C_{n_x,n_y}(t)|$ evaluated via a Cosine, Hermite, and Legendre basis. In Frame (I), there is practically no difference in the qualitative behavior of $\mathcal{L}$ for the state $(n_x, n_y) = (0, 0)$ between the different bases. $\mathcal{L}$ goes to zero in all bases and therefore chaos is absent in all of them. For $(2, 2)$, $\mathcal{L}$ is positive and close to zero. It varies slightly with bases; but it still gives the same qualitative result indicating order. For the state $(4, 4)$, the values of $\mathcal{L}$ vary with bases; but they are all positive signaling chaos.

In Frame (II), $\mathcal{L}$ for (5,2) in the Cosine basis is positive and almost constant in the time-range considered. However, for the Hermite and Legendre bases, $\mathcal{L}$ evolves from a negative towards a positive value. That is, for (5,2) $|C_{n_x,n_y}(t)|$ is eventually chaotic for all bases as $t \to \infty$. For (6,3) and (8,8), $\mathcal{L}$ displays positive values for all bases and $|C_{n_x,n_y}(t)|$ is chaotic. In Frame (III), $\mathcal{L}$ is positive in all bases for (0,0), (6,6), and (8,8). Therefore, the result of having chaos in the GP wavefunction that is basis independent can be considered as a new test for the presence of physical chaos taking into account that the three bases we are using are vastly different functions!

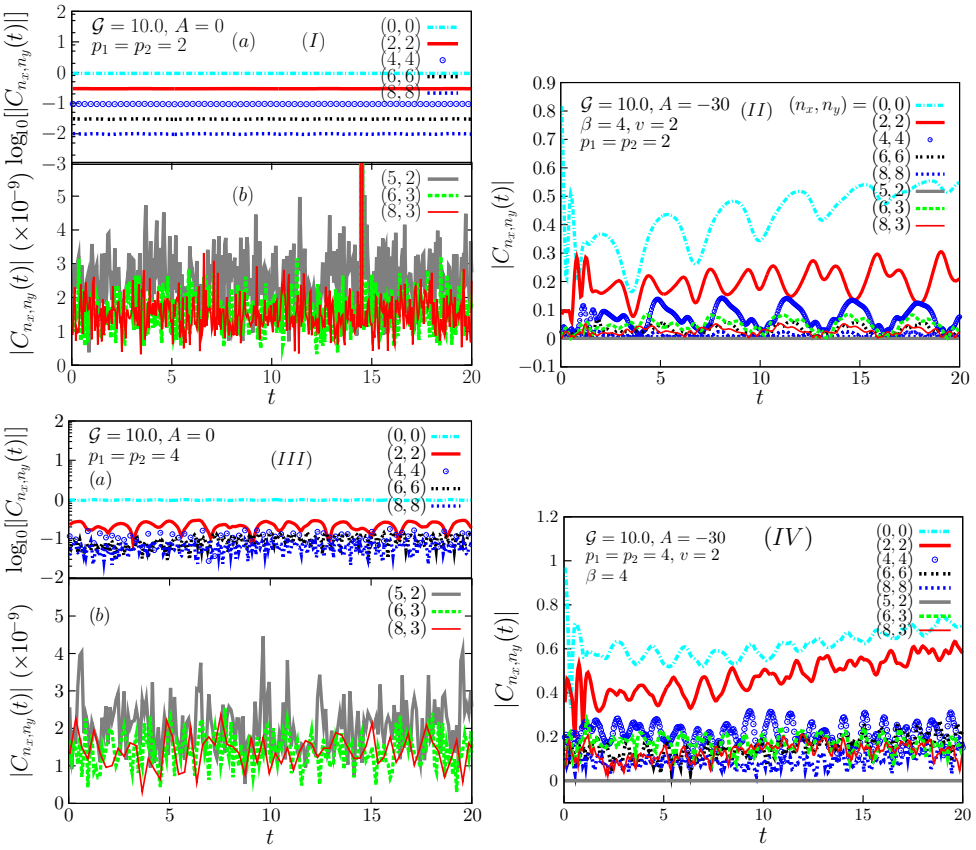

Fig. 6. Dynamics of the weights of the harmonic oscillator states, $|C_{n_x,n_y}(t)|$ of equation (15). In frame (I), the system is the same as in Figure 1; but for $A = 0$, i.e., no applied laser. Subframe (a) displays $\log_{10}[|C_{n_x,n_y}(t)|]$: dashed-dotted line: $(n_x, n_y) = (0, 0)$; solid line: $(2, 2)$; open circles: $(4, 4)$; double-dotted line: $(6, 6)$; dotted line: $(8, 8)$. Subframe (b) displays $|C_{n_x,n_y}(t)|$ in units of 10^{-9}: quadro-triple dotted line: $(5, 2)$; dashed line: $(6, 3)$; and thin solid line: $(8, 3)$. Frame (II) is the same as (I) with the same labels; but with a laser applied of parameters $A = -30$, $\beta = 4$, and $v = 2$. Frame (III) is the same as (I) with the same labels; but for $p_1 = p_2 = 4$. The lower frame (III,b) displays $|C_{n_x,n_y}(t)|$ in units of 10^{-9}. Frame (IV) is the same as (III) with the same labels; but with a laser of depth $A = -30$. A is in units of $\hbar\omega_{ho}$, $\mathcal{G}$ in $(\sqrt{2}a_{ho}^2)^{-1}$, v in a_{ho}, β in $(a_{ho})^{-2}$, and $t = \tau\omega_{ho}$ is unitless.

4.4 Chaos in coordinate space

Figure 8 further confirms the presence of spatial chaos in the coordinate space of the BEC via the evolution of $\mathcal{L}$ for R_{rms}. The computations ran for a time $t = 10\,000$, long enough to examine the asymptotic-time behavior of $\mathcal{L}$. For the upper and lower frames, the parameters of the time series analysis and the resulting asymptotic Lyapunov exponents $\mathcal{L}_{asymp}$ are listed in Tables 1 and 2, respectively. All $\mathcal{L}$ converge to stable positive values after a long simulation confirming the existence of chaos. The stability of $\mathcal{L}$ signals that once chaos has been initiated in a BEC, it does not decay if one allows the BEC to evolve for a long time. Therefore, one needs to design ways to suppress chaos, particularly if it arises in quantum computations.

4.5 Chaos in energy space

We now confirm the existence of chaos in energy space for most of the cases considered in this work. Figure 9 shows trajectories $(E, \dot{E})$ for all energy components E in addition to $(R_{rms}, \dot{R}_{rms})$ in a harmonic trap stirred by a blue-detuned laser. In this, order is categorically demonstrated in E_{kin}, E_{osc}, and R_{rms} because their trajectories display periodic behavior whereas chaos is prevalent in the other components as they are aperiodic. A trend is also revealed by all chaotic components in developing an attractor as, for example, the Rössler attractor [87,88] by E_{flow} and E_{int}. The separated-out trajectories demonstrate the state of the system while the BDLP is inside the trap.

Figure 10 in turn demonstrates that in the same harmonic trap but with red-detuned laser stirring, E_{kin} and E_{osc} are no longer ordered and the rest of the energy components remain chaotic. It is possible that R_{rms} may be spiraling into a kind of periodic behavior at longer times after exhibiting chaos. Indeed, all trajectories seem to evolve towards a concentrated dense "area" because once the RDLP leaves the BP, the number of excited states goes down as the points on the trajectories come closer together. Indeed, as can be deduced from frame (f), the volume of phase-space is reduced as the BEC evolves with time indicating a decline in the number of energy states to

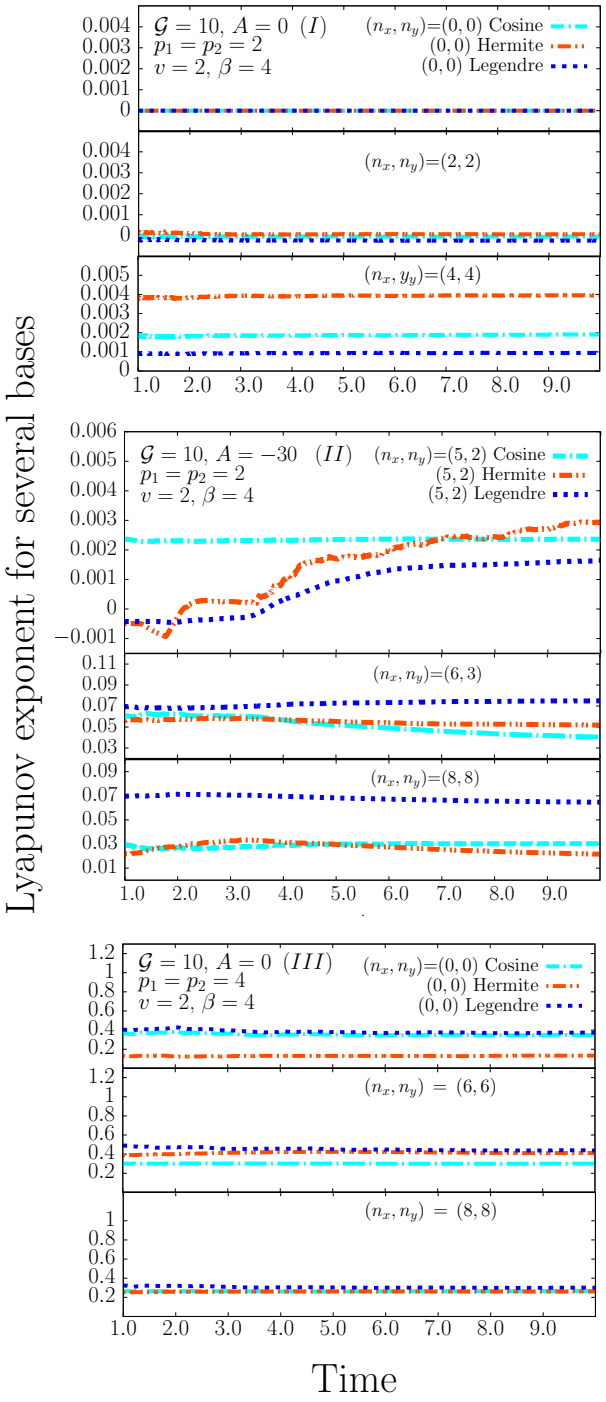

Fig. 7. Lyapunov exponents of the weights $|C_{n_x,n_y}(t)|$ (Eq. (15)) for different bases used in the expansion of the total wavefunction. The x-axis is the time t in units of 10^4. The system is in principle that of Figure 1. Frame (I) is for $A = 0$ and $p_1 = p_2 = 2$. Dashed-dotted line: cosine basis; dashed double-dotted line: Hermite; and dotted line: Legendre. Top subframe: state $(n_x, n_y) = (0, 0)$; middle: $(2, 2)$; and bottom: $(4, 4)$. Frame (II) is for $A = -30$ and $p_1 = p_2 = 2$. Legends are the same as in (I). Top frame: $(5, 2)$; middle: $(6, 3)$; bottom: $(8, 8)$. Frame (III) is for $A = 0$ and $p_1 = p_2 = 4$. Legends are again as above. Top subframe: $(0, 0)$; middle: $(6, 6)$; and bottom: $(8, 8)$. A is in units of $\hbar\omega_{ho}$, $\mathcal{G}$ in $(\sqrt{2}a_{ho}^2)^{-1}$; β in (a_{ho}^{-2}); and $t = \tau\omega_{ho}$ is unitless.

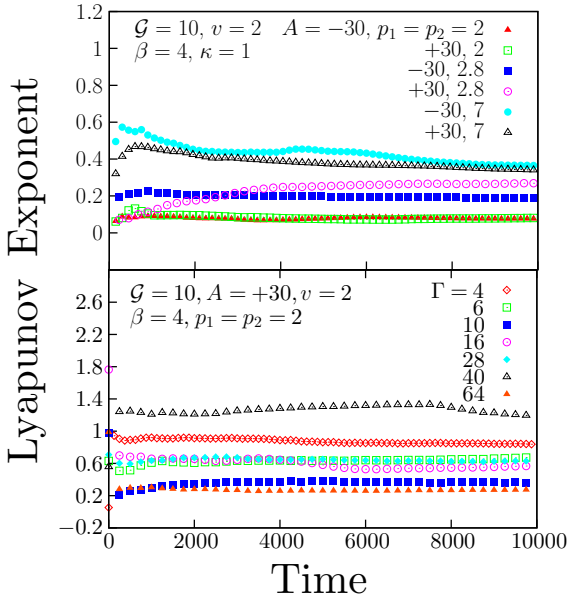

Fig. 8. Evolution of the Lyapunov exponent $\mathcal{L}$ for various systems considered from Figures 1 and 2 after a very long simulation time $t = 10\,000$. The interaction parameter is $\mathcal{G} = 10$ and the velocity of the stirrer is $v = 2$ with width parameter $\beta = 4$. Upper frame: $\mathcal{L}$ of $R_{rms}(t)$ for various values of A and $p_1 = p_2$. Solid triangles: $A = -30$, $p_1 = p_2 = 2$; open squares: $+30$, 2; solid squares: -30, 2.8; open circles: $+30$, 2.8; solid circles: -30, 7; open triangles: $+30$, 7. Lower frame: $\mathcal{L}$ at various values of Γ (cf. Eq. (18)) for $A = +30$ and $p_1 = p_2 = 2$. Open diamonds: $\Gamma = 4$; open squares: 6; solid squares: 10; open circles: 16; solid circles: 28; open triangles: 40; and solid triangles: 64. A is in units of $\hbar\omega_{ho}$, $\mathcal{G}$ in $(\sqrt{2}a_{ho}^2)^{-1}$, v in a_{ho}, β in $(a_{ho})^{-2}$, and $t = \tau\omega_{ho}$ is unitless.

Table 1. Asymptotic Lyapunov exponents $\mathcal{L}_{asymp}$ of R_{rms} for the systems of Figures 1 and 2. Parameters are: trapping exponents p_1 and p_2 and stirrer depth or height A (see Eq. (3)), optimal embedding delay τ, and minimal required dimension m. The velocity of the stirrer is $v = 2$ and the parameter describing its width is $\beta = 4$. A is in units of $\hbar\omega_{ho}$, β in a_{ho}^{-2}, and v in a_{ho}.

p_1	p_2	A	τ	m	$\mathcal{L}_{asymp}$
2	2	+20	16	5	0.056033
2	2	+30	16	5	0.081165
2	2	+40	15	5	0.081559
2	2	−20	15	5	0.280095
2	2	−30	15	5	0.076887
2	2	−40	14	5	0.015436
2.8	2.8	−30	11	7	0.188084
2.8	2.8	+30	11	7	0.268660
5	5	+30	8	7	0.099709
5	5	−30	6	7	0.619132
7	7	−30	5	7	0.365345
7	7	+30	5	7	0.339876

which the system is excited. Comparing Figures 9 and 10, one can see then that the RDLP generates chaos in E_{kin}, E_{osc}, and R_{rms} because it introduces a larger phase space

Table 2. As in Table 1; but for the systems of Figure 3 at various values of the relative constant Γ. The amplitude of the stirrer is fixed at $A = +30$ and $p_1 = p_2 = 2$. Parameters are: Γ, optimal embedding delay τ, and minimal required dimension m. A is in units of $\hbar\omega_{ho}$.

Γ	τ	m	$\mathcal{L}_{asymp}$
4	4	6	0.833164
6	3	6	0.676284
10	1	6	0.364494
16	1	6	0.571895
28	1	6	0.629997
40	1	6	1.186200
64	1	6	0.272363

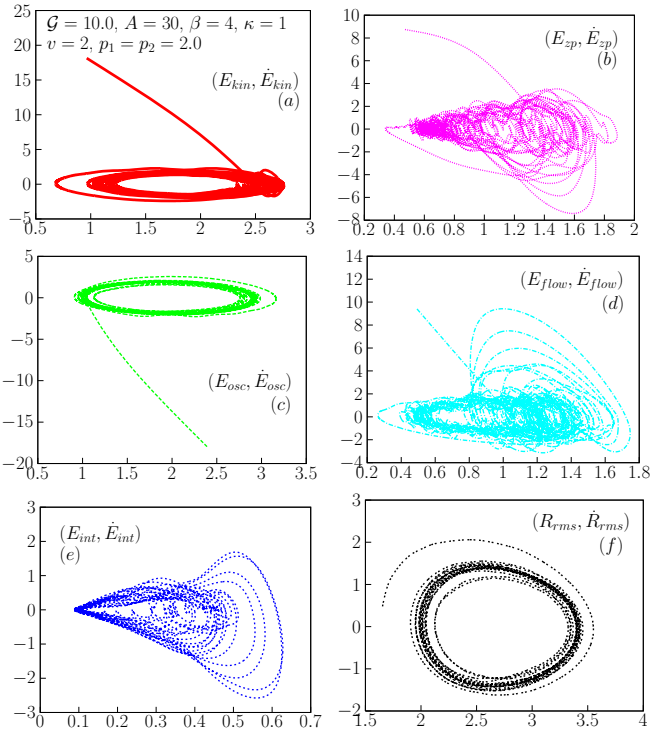

Fig. 9. Energy trajectories $(E, \dot{E})$ of the system in Figure 1c and 1d for a time of $t = 20$. Frame (a) $E = E_{kin}$; (b) E_{zp}; (c) E_{osc}; (d) E_{flow}; (e) E_{int}; and (f) additionally the phase-space trajectory $(R_{rms}, \dot{R}_{rms})$. Lengths and energies are in units of the trap, a_{ho} and $\hbar\omega_{ho}$, respectively, and t is unitless.

density. Consequently, the extent of the trajectories along both axes is larger for the red than blue-detuned laser.

In Figure 11, chaos is also signaled by all the above physical observables in an anharmonic trap with a blue-detuned laser. In this case, the trajectories probe more of the space of $(E, \dot{E})$ and a larger number of excited states is manifested than for the corresponding harmonic trap in Figure 9. This is because anharmonicity introduces a larger quantum pressure due to stronger confinement that excites the BEC to higher energy levels. In the corresponding Figure 12 with a red-detuned laser, the patterns of the trajectories are qualitatively not very different from their counterparts in Figure 11 demonstrating that the

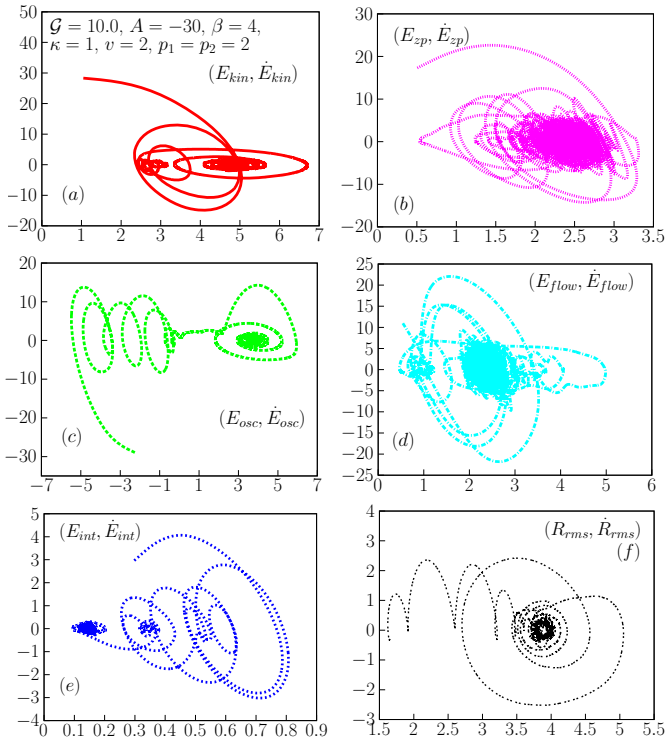

Fig. 10. As in Figure 9; but for $A = -30$ (system in Figs. 1i and 1j).

trap anharmonicity has become dominant in determining the qualitative behavior of the trajectories. The trajectories $(R_{rms}, \dot{R}_{rms})$ in Figures 11 and 12 clearly exhibit chaos as they do not form periodic orbits. Compared with the harmonic trap, the extent of these trajectories along R_{rms} is reduced, whereas along E it increases with increasing confinement strength via $p_1 = p_2$.

4.6 More quantum effects

What remains now is to examine chaos with increased Γ. Figure 13 shows the trajectories $(X, \dot{X})$ for the evolution of R_{rms}, E_{zp}, and E_{flow}. These figures verify the presence of chaos in coordinate and energy space with increased Γ because none of them manifests periodic behavior. The range of these observables and their time-derivatives rises with increasing Γ. For R_{rms}, this shows that an increased degree of chaos implies a rise in the relative sizes of the BEC and external trap. One can also ascribe to this behavior an artificial rise in the "volume" of phase-space that signals an increase in the number of energy states. This is further supported by an increase in the range of E_{zp} and E_{flow} (and their derivatives).

4.7 Confirmation of energy chaos via the Lyapunov exponent

The aim now is to apply the Lyapunov exponent as a measure that further confirms the presence or absence of

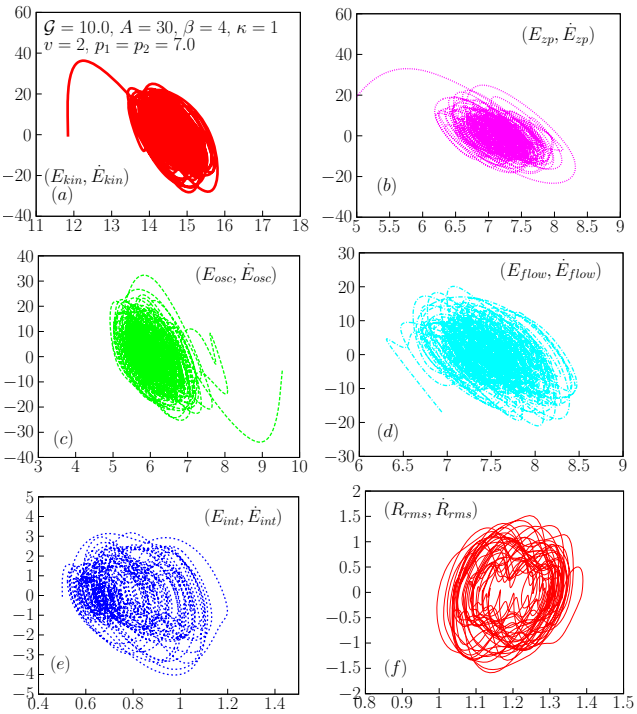

Fig. 11. As in Figure 9; but for $p_1 = p_2 = 7$ (system in Figs. 2e and 2f).

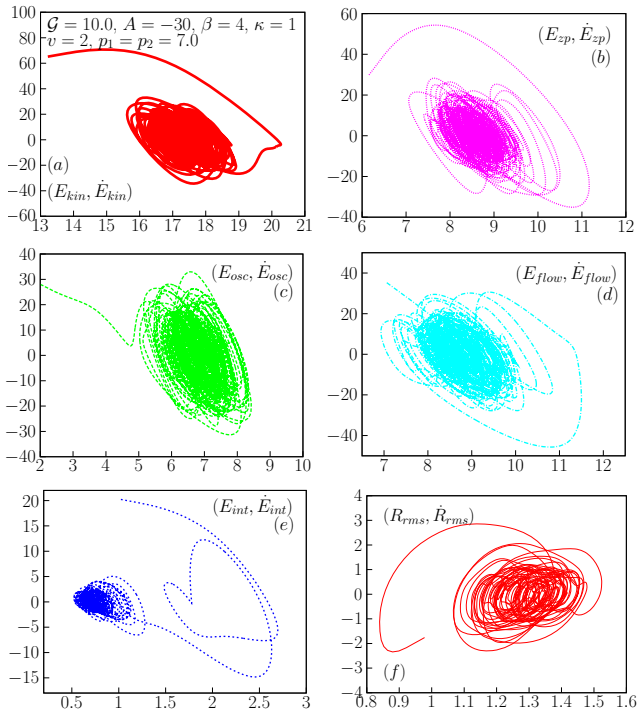

Fig. 12. As in Figure 10; but for $p_1 = p_2 = 7$ (system in Figs. 2k and 2l).

chaos and how long it persists in the BEC. In Figure 14, the evolution of $\mathcal{L}$ for the energy components is displayed. Scanning all frames, it can be seen that after a long simulation time $\mathcal{L}$ is positive for all the observables under consideration; except in frame (K). However, it was found hard to assign a certain behavioral pattern for $\mathcal{L}$ in terms of trapping geometry and laser parameters. For a harmonically trapped BEC that is excited by a red-detuned laser, $\mathcal{L}$ for the energies seems to approach stable values, except for E_{zp} where $\mathcal{L}$ declines after $t \sim 2000$. This decline is an indication that the degree of chaos in E_{zp} decreases with time. Similarly, with a blue-detuned laser, the $\mathcal{L}$'s stabilize with time except for E_{flow} and E_{int}, which keep rising, and with it the degree of chaos in them. For anharmonic trapping with a red- or blue-detuned laser, there is no qualitative change in the behavior of $\mathcal{L}$ when compared with the corresponding harmonic trapping. For some of the observables, the values of $\mathcal{L}$ are significantly larger than for the harmonic trapping. For example, in frame (F), $\mathcal{L}$ for E_{kin} reaches $\sim$3.6 whereas in frame (B) it is $\sim$0.2 for the same blue-detuned laser. In frame (E), $\mathcal{L}$ for E_{flow} reaches $\sim$4.6 compared with $\sim$3.5 in frame (A) for the same red-detuned laser, and similarly for other observables. Over some energy intervals, chaos arises with increasing trapping anharmonicity bringing this in line with the behavior of energy trajectories in Figures 9–12. Frames (G) and (H) present the same qualitative information as in frame (B) with different blue-detuned laser amplitudes. Nevertheless, some predictability can be assigned to the response of the magnitude of $\mathcal{L}$ to increasing quantum effects. $\mathcal{L}$ for E_{flow} and E_{zp} is seen to rise with increasing Γ beyond 1. In contrast, with $\Gamma \ll 1$, $\mathcal{L}$ tends to approach zero except for E_{osc} where $\mathcal{L}$ becomes negative signalling the absence of chaos. This is brought in line with observations in Figures 4a and 4b. Therefore, the reduction of quantum effects leads to ordered behavior in physical observables. The chaotic behavior remains in general unpredictable. From the previous displays, one concludes that chaos persists for a very long time and does not easily vanish in nondissipative systems.

4.8 Analogy to the chaotic billiard

The spatial chaos and order found in Figures 1 and 2 can be explained by the chaotic billiard concept [31] whose effects can be mimicked by an anharmonic trap. In 2D, the trajectories of a particle moving with constant energy on a billiard table with defocusing boundaries are chaotic unlike one that has a circular-shaped boundary [31]. For a harmonic trap in 2D, the BEC with low kinetic energy is unable to surmount the barrier of the external trap and remains therefore far away from the BP hard walls. Accordingly, it oscillates periodically inside a circular area and endures no chaotic billiard effect. If the energy is increased, the BEC oscillates within a larger circular area which if cutoff by the BP becomes, for certain energy levels, square-like with rounded corners. By increasing the energy, the BEC moves up the potential barrier of the external trap and eventually becomes a squared area. After this, it no longer oscillates periodically. For an anharmonic trap, the shape of the spatial boundary is not circular as for a harmonic trap, but square-like with rounded corners and becomes square with increasing anharmonicity.

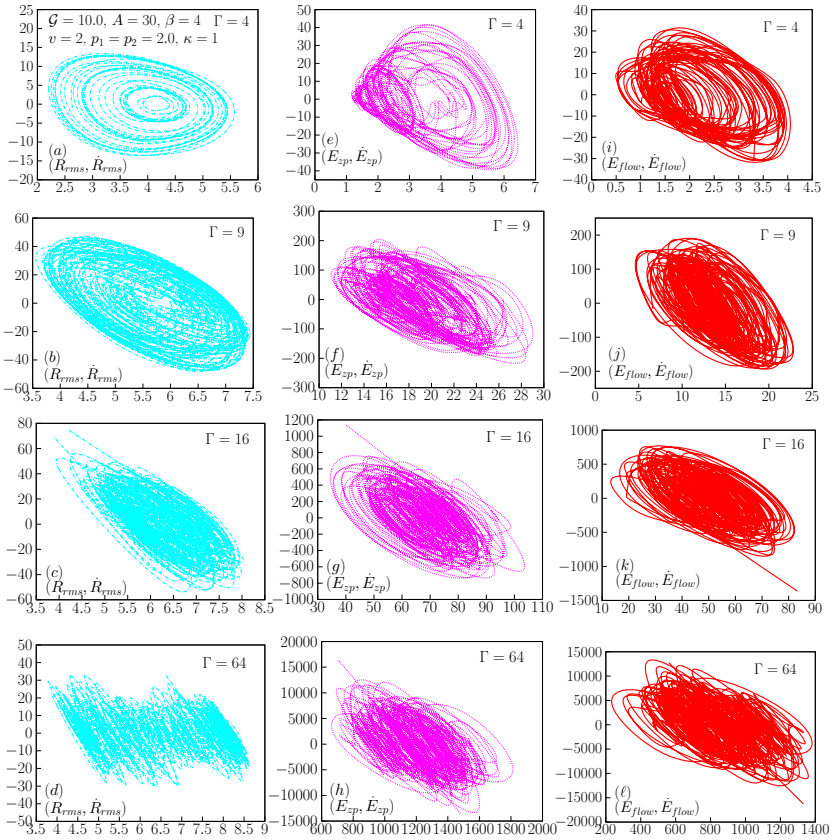

Fig. 13. Quantum effects revealed by the phase-space and energy trajectories for the system of Figure 3. In all frames, the relative Planck's constant Γ is increased from top to bottom according to the sequence 4, 9, 16, and 64. Left column (frames (a)–(d)): phase-space trajectories $(R_{rms}, \dot{R}_{rms})$; middle column (frames (e)–(h)): zero-point energy trajectories $(E_{zp}, \dot{E}_{zp})$; right column (frames (i)–(l)): kinetic-flow energy trajectories $(E_{flow}, \dot{E}_{flow})$. $R_{rms}(t)$ is in units of a_{ho} and $E_{zp}(t)$ and E_{flow} are in units of $\hbar\omega_{ho}/\sqrt{\Gamma}$.

Therefore, the dynamics of the BEC becomes chaotic with a broad excitation spectrum and spatial chaos increases with growing anharmonicity. One understands now why there is spatial order for a blue-detuned laser: for the BDLP parameters considered, the BEC is not excited to energy levels where the BP begins to be assertive; the BEC remains therefore inside a circular boundary and oscillates periodically. In contrast, the RDLP excites the BEC to high energy levels where the BP begins to be assertive.

5 Validity of the GPE in the present approach

Our use of the GPE is justified (1) by the success of previous similar work [42,43,47,55,89], (2) because the temperature remains in a regime well below the critical temperature T_c, and (3) because the scattering length $a_s \ll \overline{d}$, where $\overline{d} = \sqrt{L^2/N} = 2.81$ μm is less than the average interparticle separation; i.e., our systems are very dilute Bose gases. Regarding (1), Fujimoto and Tsubota (FT) [43] examined the dynamics of a trapped BEC induced by an oscillating Gaussian potential. Their study was based on a numerical simulation of the 2D GPE. Because it was thought that the oscillating potential might induce some heating effects that might invalidate their use of the GPE, they calculated the increase of temperature and showed that it remained relatively very small.

Further support for our arguments can be drawn from the work of reference [90], where a quasipure condensate was identified because it constituted a fraction of only 77%. In addition, the GPE was applied to explore BECs excited by obstacles. For example, Sasaki et al. [89] explored vortex shedding from an obstacle moving inside the BEC. Horng et al. [55] examined the dynamics of turbulent flow in a 2D trapped BEC. Caradoc-Davis et al. [47] simulated the effects of rotationally stirring a 3D trapped BEC with a Gaussian laser beam.

Concerning point (2), FT used the specific-heat equation of the 2D ideal trapped Bose gas written:

$$C(T) = \frac{6k_B^3 T^3 \xi(3)}{\hbar^2 \omega_x \omega_y}, \tag{22}$$

to estimate the heating of their condensate (here $\xi(n)$ is the Riemann Zeta function with $\xi(3) = 1.2021$). This was simply obtained from a division of the energy rise ΔE by the value of $C(T)$ at the transition temperature T_c. Because our systems are dilute ($N \sim 117$, $a_s \ll \overline{d}$) and weakly-interacting, we can follow FT and apply

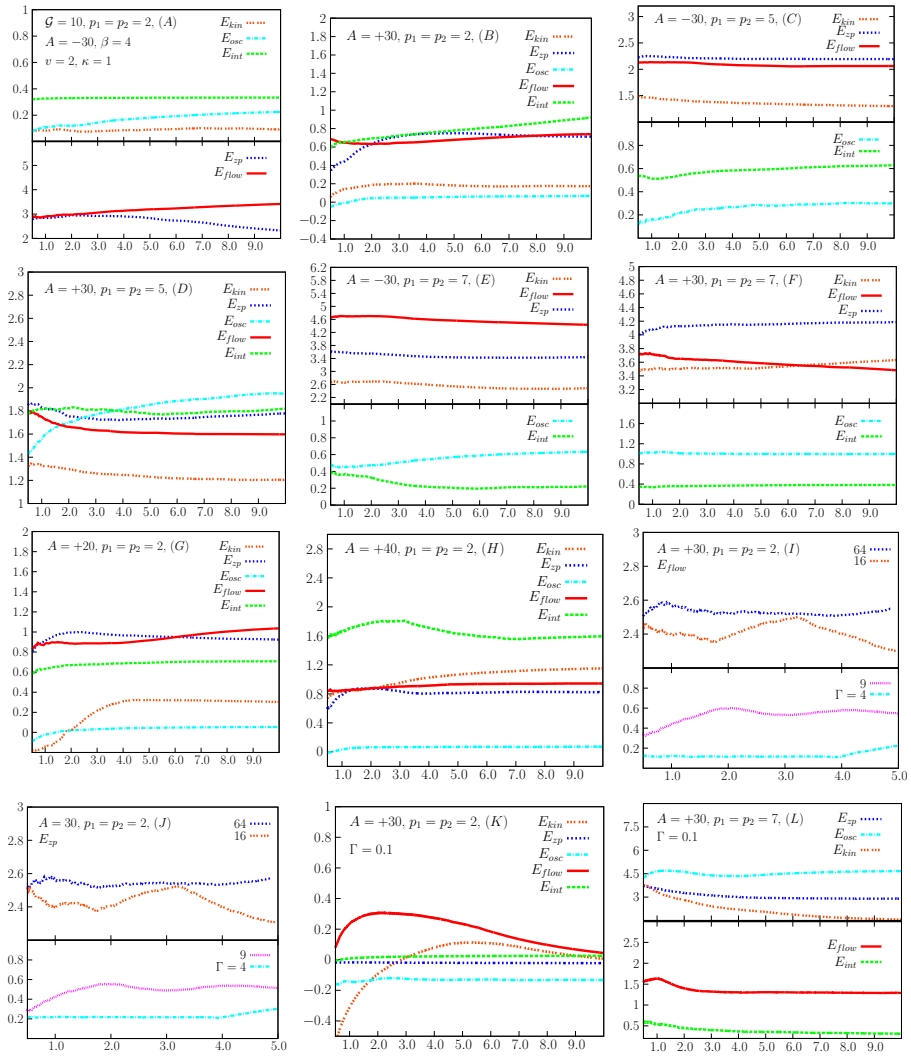

Fig. 14. Lyapunov exponents for the energy dynamics of all the previous systems in Figures 1–3 as a function of evolution time. Energy is along the y-axis and time along the x-axis. $\mathcal{G} = 10$, $v = 2$, $\beta = 4$ and $\kappa = 1$. Frame (A): $A = -30$, $p_1 = p_2 = 2$; (B) +30, 2; (C) −30, 5; (D) +30, 5; (E) −30, 7; (F) +30, 7; (G) 20, 2; (H) +40, 2. Frames (I) and (J) display the effects of increasing the relative Planck's constant Γ for $A = +30$ and $p_1 = p_2 = 2$. Dotted line: $\Gamma = 64$; triple-dotted line: 16; fine-dotted line: 9; and dashed-dotted line: 4. Frames (K) and (L) display the reduced quantum effects with $\Gamma = 0.1$. Frame (K) $A = +30$, $p_1 = p_2 = 2$; (L) 30, 7. Frames (A–H), (K), and (L) all have the same labels although the locations of the observables in the frames tend to vary: triple-dotted line: E_{kin}; dashed-dotted line: E_{osc}; dashed line: E_{int}; dotted line: E_{zp}; solid line: E_{flow}. The time is in units of 10^4.

equation (22) to estimate the temperature of our systems in the excited state only after the stirrer has left the BP. First of all, for our harmonically trapped BEC without excitation by any laser, the energy per particle is $E(A = 0) = 1.3340$ $(\hbar\omega_{ho})$; for the same system, but applying a stirring laser ($A = -30$) the energy per particle is $E(A = -30) = 8.709$ $(\hbar\omega_{ho})$. Now the difference in energies is $\Delta E = E(A = -30) - E(A = 0) = 7.375$ $(\hbar\omega_{ho})$, which is equivalent to $\Delta E = 7.375\hbar\omega_{ho} = 1.216 \times 10^{-31}$ J per particle; a value much smaller than that of FT. Second, the change in temperature from an initial value T_0 can be estimated from

$$\Delta T = T - T_0 = \frac{N\Delta E}{C(T_c)}, \tag{23}$$

where T_c is substituted into equation (22). It is recalled that T_c for the ideal 2D BEC in a harmonic trap is given by [82]

$$T_c = \frac{\hbar\omega_{ho}}{k_B}\sqrt{\frac{N}{\xi(2)}}, \tag{24}$$

with k_B Boltzmann's constant and $\xi(2) = 1.6449$. For $N \sim 117$, $T_c = 10.12$ nK. Considering $\omega_x = \omega_y = \omega_{ho}$ and that $T_0 = 0$, one gets $\Delta T = T = 2.018$ nK. The condensate fraction is then estimated from

$$N = N_0\left(1 - \frac{T^2}{T_c^2}\right), \tag{25}$$

and is equivalent to $N/N_0 = 0.96$. Therefore, our T is indeed small. See, for example Neely et al. [48] and Onofrio

et al. [50] where temperatures of $T = 52$ nK and $T = 10$ nK, respectively, were reported.

There exist methods for beyond mean-field examinations of BEC dynamics in the group of L. Cederbaum, e.g. by Březinová et al. [24] who explored the expansion of a BEC in shallow 1D potentials using the TDGPE and the multi-configurational time-dependent Hartree for bosons (MCTDHB) [91] methods. It has been shown, that the onset of wave chaos in the GPE can be used as an indication for condensate depletion. The authors particularly focused on the case where the condensate depletion is relatively weak $\lesssim 5\%$. So far, it is known that as condensate depletion increases, the GPE becomes less valid as one faces a many-body problem beyond the GPE. However, Březinová et al. made a comparison between the dynamics of the GPE and the MCTDHB and revealed that the mean-field effect of wave chaos – i.e., the buildup of random fluctuations – corresponds to the many-body effect of condensate depletion. An important and surprising finding has been that there is good agreement between expectation values of observables obtained by GPE and MCTDHB, such as the width of the cloud and the kinetic energy. It has been further found, that the GPE can mimick excitations out of the condensate, and although the depletion lies outside the range of GPE applicability, one can monitor the onset of depletion by the onset of wave chaos within GPE, a fact that extends the range of GPE applicability. Further work involving beyond-the-GPE treatments has been presented, e.g., by Billam et al. [35,36] in which a second-order number-conserving numerical method has been applied to solve the equations of motion involving a coupling between the condensate and noncondensate. Their goal was to explore finite-temperature BEC dynamics and their method has been successfully applied to the δ-kicked rotor BEC.

6 Summary and conclusions

In summary, conditions have been obtained under which order and chaos appear in the dynamics of interacting trapped Bose gases. This work has specifically distinguished chaos in coordinate space from that in energy space. The chief result is that either quantum effects or trap anharmonicity is a generator of chaos in energy space. This conclusion has been reached through an artificial variation of the relative Planck's constant Γ to values smaller or larger than 1 following reference [16]. A second important result is that chaos has been confirmed in the energy space of an excited trapped BEC. For severely reduced quantum effects ($\Gamma \ll 1$) in the presence of an external harmonic trap, no chaos is observed in either coordinate or energy space. Therefore, one way of suppressing chaos is by increasing the characteristic scale associated with the external trap with respect to the condensate size. Therefore, trap harmonicity in the absence of quantum effects is a generator of complete order in the physical observables. The presence of an external anharmonic trap and severely reduced quantum effects yields chaos in energy space, but not in coordinate space. The same happens in the presence of quantum effects ($\Gamma = 1$) and trap harmonicity. Therefore, to obtain chaos in coordinate space, both quantum effects (with $\Gamma > 1$) and trap anharmonicity (with $p_1 = p_2 > 1$) must be present. This can also be inferred from Table 3, which turns out to be similar to the logic-OR table. It is noted that, even if chaos exists in the energy space of a trapped BEC, it does not necessarily translate to chaos in coordinate space. Likewise, order in coordinate space does not imply order in energy space.

Table 3. Overview of conditions for order and chaos in coordinate (RMS radius $\sqrt{\langle r^2\rangle}$) and energy ($\langle E\rangle$) space under the possibility of an artificial variation of the relative Planck's constant [$\Gamma = (\hbar_0/\hbar)^2$] following reference [16]. The system is a BEC in an external trap cut off by a hard-wall BP boundary. It is excited by a stirring laser (see main text). From left to right, the table lists conditions: QE?= quantum effects?, TA?= trap anharmonicity?, and the results for the presence or absence of chaos in both spaces. Answers are either yes (Y) or no (N).

QE?	TA?	Chaos $\sqrt{\langle r^2\rangle}$?	Chaos $\langle E\rangle$?
N	N	N	N
N	Y	N	Y
Y	N	N	Y
Y	Y	Y	Y

Other results are as follows:

1. The non-periodic trajectories of $\dot{X}$ vs X (X being any physical quantity) supported by positive Lyapunov exponents are manifestations of chaos in the physical observables.
2. The frequency of oscillation of a property X is primarily determined by the external trap. In the presence of a stirring blue-detuned laser, this frequency is not affected, whereas a stirring red-detuned laser changes the frequency. A dynamically changing effective trapping frequency is found to be a source of chaos in the BEC.
3. While the stirring laser is inside the trap, this situation could be viewed as an initial condition. If one considers measuring these systems after the removal of the stirrer, then one can think of different initializations according to whether there was a stirring BDLP or RDLP. Inspecting the post-stirring dynamics in Figure 1, one can infer that these systems are able to *remember* the kind of laser potential used to excite them. It turns out that the dynamics of the BEC is determined according to its *history* of excitations. As the trajectories that a chaotic system follows are sensitive to initial conditions [8,31], then this further confirms that our systems are indeed chaotic.

The usefulness of the present work is that: (1) it looks deeper into the chaotic dynamics of a BEC by looking at the dynamics of the energy components; (2) the ideas presented here can be used to gain further understanding of other analogous complex systems, such as the recently achieved photonic BEC [92]; (3) it should motivate the exploration of chaos excited by other methods,

such as an oscillating stirrer [42,43,50,53] and a rotational one [46,47,52,54].

The authors thank the Abdus Salam International Center for Theoretical Physics in Trieste, Italy for a hospitable stay during which part of this work was undertaken. ARS thanks the Max Planck Institute for Physics of Complex systems (MPIPKS) in Dresden Germany for a hospitable stay and for providing access to their excellent computing facilities on which most of the current simulations were performed. Stimulating and enlightening discussions with Soskin Stanislav (Lancaster University, UK) and Rajat Karnatak (MPIPKS Dresden, Germany) are gratefully acknowledged. This work was undertaken during sabbatical leave granted to the author Asaad R. Sakhel from Al-Balqa Applied University (BAU) during academic year 2014/2015. AB acknowledges financial support by the Ministry of Education, Science, and Technological Development of the Republic of Serbia under project ON171017.

Appendix: Effective trapping frequency

The trapping frequencies ω_x and ω_y of the combined external+laser trap $\tilde{V}(x,y;t)$, equation (3), are given by:

$$\omega_q(x,y;t) = \sqrt{\frac{\partial^2 \tilde{V}(x,y;t)}{\partial q^2}}, \tag{A.1}$$

where $q \equiv (x,y)$ and ω_q is therefore a function of the coordinates. However, these equations are only valid near the minima of $\tilde{V}(x,y;t)$. Substituting equation (3) into equation (A.1) yields

$$\omega_x(x,y;t) = \left\{ \frac{\sigma}{4} p_1(p_1-1)|x|^{p_1-2} - 2\beta A(1-2\beta x^2) \times \exp[-\beta(x^2+(y-vt)^2)] \right\}^{1/2}, \tag{A.2}$$

and

$$\omega_y(x,y;t) = \left\{ \frac{\sigma}{4} p_2(p_2-1)|y|^{p_2-2} - 2\beta A[1-2\beta(y-vt)^2] \times \exp[-\beta(x^2+(y-vt)^2)] \right\}^{1/2}. \tag{A.3}$$

Hence, ω_x and ω_y are controlled by the overall shape of the combined trap and particularly the height or depth of the applied laser potential. Note that for $A<0$, ω_x and ω_y will increase with "increasing" $A<0$. If $A>0$, the frequencies decrease.

By setting $p_1 = p_2 = 2$, one obtains for a harmonic trap

$$\omega_x(x,y;t) = \left\{ \frac{\sigma}{2} - 2\beta A(1-2\beta x^2) \exp[-\beta(x^2+(y-vt)^2)] \right\}^{1/2}, \tag{A.4}$$

and

$$\omega_y(x,y;t) = \left\{ \frac{\sigma}{2} - 2\beta A[1-2\beta(y-vt)^2] \exp[-\beta(x^2+(y-vt)^2)] \right\}^{1/2}. \tag{A.5}$$

Note that in this case, the spatial variations of the combined trap ruling ω_q arise only from the laser potential because those due to the harmonic trap have been eliminated!

A.1 Red-detuned Laser

At $t=0$, the only minimum in the combined harmonic trap is found at $x=y=0$ at the bottom of the RDLP well. Therefore

$$\omega_x(0,0;0) = \omega_y(0,0;0) = \left[\frac{\sigma}{2} - 2\beta A\right]^{1/2}. \tag{A.6}$$

At $t>0$, when the laser has moved only a little, such that there is still only one minimum in the combined trap, one gets at $x=0$ and $y=vt$ the same ω_x and ω_y as in equation (A.6), i.e.,

$$\omega_x(0,vt;t) = \omega_y(0,vt;t) = \left[\frac{\sigma}{2} - 2\beta A\right]^{1/2}. \tag{A.7}$$

As long as there is only one minimum (that of the RDLP), ω_x and ω_y will remain constant at all times t. However, when the red-detuned laser has moved far enough from the center of the harmonic trap, another minimum arises at $x=y=0$. Here, the frequencies become time-dependent with values given by:

$$\omega_x(0,0;t) = \left\{ \frac{\sigma}{2} - 2\beta A \exp[-\beta v^2 t^2] \right\}^{1/2}, \tag{A.8}$$

and

$$\omega_y(0,0;t) = \left\{ \frac{\sigma}{2} - 2\beta A[1-2\beta v^2 t^2] \exp[-\beta v^2 t^2] \right\}^{1/2}. \tag{A.9}$$

Hence the frequency of BEC-density oscillations inside the trap is subject to change with time, and this tends to be one source of chaos in these oscillations. Inside the reference frame of the RDLP, the BEC oscillates at a fixed frequency when $p_1 = p_2 = 2$.

For the anharmonic trap, say with $p_1 = p_2 = 7$, at the minimum of the RDLP $x=y=0$, one obtains for $t=0$

$$\omega_x(0,0;0) = \omega_y(0,0;0) = \sqrt{-2\beta A}, \tag{A.10}$$

and similarly for $t>0$

$$\omega_x(0,vt;t) = \omega_y(0,vt;t) = \sqrt{-2\beta A}. \tag{A.11}$$

When the RDLP has moved far away from $x=y=0$, there arises a minimum at the center of the anharmonic

trap with trapping frequencies

$$\omega_x(0,0;t) = \sqrt{-2\beta A}\exp\left(-\frac{1}{2}\beta v^2 t^2\right),$$
$$\omega_y(0,0;t) = \sqrt{-2\beta A(1-2\beta v^2 t^2)}\exp\left(-\frac{1}{2}\beta v^2 t^2\right), \tag{A.12}$$

and inside the RDLP

$$\omega_y(0,vt;t) = \left[10.5\sigma|vt|^5 - 2\beta A\right]^{1/2},$$
$$\omega_x(0,vt;t) = \sqrt{-2\beta A}. \tag{A.13}$$

A.2 Blue-detuned laser

In this case for a harmonic trap at $t = 0$, we have a maximum at $x = y = 0$, and there exists a minimum along a circular region around the barrier of $\tilde{V}(x,y;t)$. Assuming that this circle of minima has a radius r_0, then $x_0^2+y_0^2 = r_0^2$ and $t = 0$ yield

$$\omega_x(x_0,y_0;0) = \left\{\frac{\sigma}{2} - 2\beta A(1-2\beta x_0^2)\exp[-\beta r_0^2]\right\}^{1/2}, \tag{A.14}$$

and

$$\omega_y(x_0,y_0;0) = \left\{\frac{\sigma}{2} - 2\beta A(1-2\beta y_0^2)\exp[-\beta r_0^2]\right\}^{1/2}. \tag{A.15}$$

When the BDLP moves, the previous circle of minima will vanish, and once the BDLP is far enough from the center of the harmonic trap the minimum at $x = y = 0$ reappears. There is still a second minimum between the BDLP and the BP when viewed along the y-direction. If this minimum is located at y_0 and time t, then it is possible that this minimum with trapping frequency

$$\omega_y(0,y_0;t) = \left\{\frac{\sigma}{2} - 2\beta A[1-2\beta(y_0-vt)^2] \times \exp[-\beta(y_0-vt)^2]\right\}, \tag{A.16}$$

could provide some trapping at y_0 along y. However, in the x-direction equation (A.1) no longer applies for this case. The latter extremum is a saddle point with negative curvature in the x-direction and positive curvature in the y-direction.

References

1. S. Kodba, M. Perc, M. Marhl, Eur. J. Phys. **26**, 205 (2005)
2. V.S. Filho, A. Gammal, T. Frederico, L. Tomio, Phys. Rev. A **62**, 033605 (2000)
3. B. Gertjerenken, S. Arlinghaus, N. Teichmann, C. Weiss, Phys. Rev. A **82**, 023620 (2010)
4. P. Muruganandam, S.K. Adhikari, Phys. Rev. A **65**, 043608 (2002)
5. H. Xiong, B. Wu, Phys. Rev. A **82**, 053634 (2010)
6. N. Katz, O. Adam, New J. Phys. **12**, 073020 (2010)
7. G. Chong, W. Hai, Q. Xie, Chaos **14**, 217 (2004)
8. I. Brezinová, L.A. Collins, K. Ludwig, B.I. Schneider, J. Burgdörfer, Phys. Rev. A **83**, 043611 (2011)
9. S. Tomsovic, E.J. Heller, Phys. Rev. Lett. **67**, 664 (1991)
10. M. Diver, G.R.M. Robb, G.-L. Oppo, Phys. Rev. A **89**, 033602 (2014)
11. A. Jaouadi, N. Gaaloul, B. Viaris de Lesegno, M. Telmini, L. Pruvost, E. Charron, Phys. Rev. A **82**, 023613 (2010)
12. Qianquan Zhu, Wenhua Hai, Shiguang Rong, Phys. Rev. E **80**, 016203 (2009)
13. J. Martin, B. Georgeot, D.L. Shepelyansky, Phys. Rev. E **79**, 066205 (2009)
14. E. Horsely, S. Koppell, L.E. Reichl, Phys. Rev. E **89**, 012917 (2014)
15. P. Coullet, N. Vandenberghe, Phys. Rev. E **64**, 025202(R) (2001)
16. A. Kapulkin, A.K. Pattanayak, Phys. Rev. Lett. **101**, 074101 (2008)
17. Jing Zhang, Yu-Xi Liu, Wei-Min Zhang, Lian-Ao Wu, Re-Bing Wu, Tzyh-Jong Tarn, Phys. Rev. B **84**, 214304 (2011)
18. W. Vincent Liu, W.C. Schieve, Phys. Rev. Lett. **78**, 3278 (1997)
19. D.S. Brambila, A. Fratalocchi, Sci. Rep. **3**, 1 (2013)
20. A. Brandstäter, J. Swift, H.L. Swinney, A. Wolf, T. Doyne Farmer, P.J. Crutchfield, Phys. Rev. Lett. **51**, 1442 (1983)
21. S.A. Gardiner, J. Mod. Opt. **49**, 1971 (2002)
22. Jing Cheng, Phys. Rev. A **81**, 023619 (2010)
23. Wenhua Hai, Shiguang Rong, Qianquan Zhu, Phys. Rev. E **78**, 066214 (2008)
24. I. Brezinová, A.U.J. Lode, A.I. Streltsov, O.E. Alon, L.S. Cederbaum, J. Burgdörfer, Phys. Rev. A **86**, 013630 (2012)
25. B. Lévi, B. Georgeot, D.L. Shepelyansky, Phys. Rev. E **67**, 046220 (2003)
26. B. Georgeot, D.L. Shepelyansky, Phys. Rev. E **62**, 3504 (2000)
27. C. Weitenberg, S. Kuhr, K. Mølmer, J.F. Sherson, Phys. Rev. A **84**, 032322 (2011)
28. J.K. Pachos, P.L. Knight, Phys. Rev. Lett. **91**, 107902 (2003)
29. V. Milner, J.L. Hanssen, W.C. Campbell, M.G. Raizen, Phys. Rev. Lett. **86**, 1514 (2001)
30. Chuanwei Zhang, Jie Liu, M.G. Raizen, Qian Niu, Phys. Rev. Lett. **92**, 054101 (2004)
31. S. Wimberger, *Nonlinear Dynamics and Quantum Chaos* (Springer Int. Pub., Switzerland, 2014)
32. R. Chacón, D. Bote, R. Carretero-González, Phys. Rev. E **78**, 036215 (2008)
33. Y. Castin, R. Dum, Phys. Rev. Lett. **79**, 3553 (1997)
34. S.A. Gardiner, D. Jaksch, R. Dum, J.I. Cirac, P. Zoller, Phys. Rev. A **62**, 023612 (2000)
35. T.P. Billam, S.A. Gardiner, New J. Phys. **14**, 013038 (2012)
36. T.P. Billam, P. Mason, S.A. Gardiner, Phys. Rev. A **87**, 033628 (2013)
37. Jie Liu, Chuanwei Zhang, M.G. Raizen, Qian Niu, Phys. Rev. A **73**, 013601 (2006)
38. L. Fallani, L. De Sarlo, J.E. Lye, M. Modugno, R. Saers, C. Fort, M. Inguscio, Phys. Rev. Lett. **93**, 140406 (2004)
39. A.J. Ferris, M.J. Davis, R.W. Geursen, P. Blair Blakie, A.C. Wilson, Phys. Rev. A **77**, 012712 (2008)

40. M.C. Garrett, A. Ratnapala, E.D. van Ooijen, C.J. Vale, K. Weegink, S.K. Schnelle, O. Vainio, N.R. Heckenberg, H. Rubinsztein-Dunlop, M.J. Davis, Phys. Rev. A **83**, 013630 (2011)
41. J.S. Stießberger, W. Zwerger, Phys. Rev. A **62**, 061601(R) (2000)
42. K. Fujimoto, M. Tsubota, Phys. Rev. A **82**, 043611 (2010)
43. K. Fujimoto, M. Tsubota, Phys. Rev. A **83**, 053609 (2011)
44. B. Jackson, J.F. McCann, C.S. Adams, Phys. Rev. A **61**, 051603(R) (2000)
45. A. Radouani, Phys. Rev. A **70**, 013602 (2004)
46. B.M. Caradoc-Davies, R.J. Ballagh, K. Burnett, Phys. Rev. Lett. **83**, 895 (1999)
47. B.M. Caradoc-Davies, R.J. Ballagh, P.B. Blakie, Phys. Rev. A **62**, 011602(R) (2000)
48. T.W. Neely, E.C. Samson, A.S. Bradley, M.J. Davis, B.P. Anderson, Phys. Rev. Lett. **104**, 160401 (2010)
49. P. Engels, C. Atherton, Phys. Rev. Lett. **99**, 160405 (2007)
50. R. Onofrio, C. Raman, J.M. Vogels, J.R. Abo-Shaeer, A.P. Chikkatur, W. Ketterle, Phys. Rev. Lett. **85**, 2228 (2000)
51. K.W. Madison, F. Chevy, W. Wohlleben, J. Dalibard, Phys. Rev. Lett. **84**, 806 (2000)
52. C. Raman, J.R. Abo-Shaeer, J.M. Vogels, K. Xu, W. Ketterle, Phys. Rev. Lett. **87**, 210402 (2001)
53. C. Raman, M. Köhl, R. Onofrio, D.S. Durfee, C.E. Kuklewicz, Z. Hadzibabic, W. Ketterle, Phys. Rev. Lett. **83**, 2502 (1999)
54. K.W. Madison, F. Chevy, V. Bretin, J. Dalibard, Phys. Rev. Lett. **86**, 4443 (2001)
55. T.-L. Horng, S.-C. Gou, T.-C. Lin, G.A. El, A.P. Itin, A.M. Kamchatnov, Phys. Rev. A **79**, 053619 (2009)
56. N.P. Proukakis, J. Schmiedmayer, H.T.C. Stoof, Phys. Rev. A **73**, 053603 (2006)
57. R.B. Diener, B. Wu, M.G. Raizen, Qian Niu, Phys. Rev. Lett. **89**, 070401 (2002)
58. T. Aioi, T. Kadokura, T. Kishimoto, H. Saito, Phys. Rev. X **1**, 021003 (2011)
59. H. Uncu, D. Tarhan, E. Demiralp, Ö. Müstecaplioğlu, Laser Phys. **18**, 331 (2008)
60. A.V. Carpentier, J. Belmonte-Beitia, H. Michinel, M.I. Rodas-Verde, J. Mod. Opt. **55**, 2819 (2008)
61. M. Hammes, D. Rychtarik, H.-C. Nägerl, R. Grimm, Phys. Rev. A **66**, 051401(R) (2002)
62. D.R. Scherer, C.N. Weiler, T.W. Neely, B.P. Anderson, Phys. Rev. Lett. **98**, 110402 (2007)
63. C. Tuchendler, A.M. Lance, A. Browaeys, Y.R.P. Sortais, P. Grangier, Phys. Rev. A **78**, 033425 (2008)
64. D.M. Stamper-Kurn, H.-J. Miesner, A.P. Chikkatur, S. Inouye, J. Stenger, W. Ketterle, Phys. Rev. Lett. **81**, 2194 (1998)
65. D. Comparat, A. Fioretti, G. Stern, E. Dimova, B. Laburthe Tolra, P. Pillet, Phys. Rev. A **73**, 043410 (2006)
66. D. Jacob, E. Mimoun, L. De Sarlo, M. Weitz, J. Dalibard, F. Gerbier, New J. Phys. **13**, 065022 (2011)
67. T.L. Gustavson, A.P. Chikkatur, A.E. Leanhardt, A. Görlitz, S. Gupta, D.E. Pritchard, W. Ketterle, Phys. Rev. Lett. **88**, 020401 (2001)
68. M.D. Barrett, J.A. Sauer, M.S. Chapman, Phys. Rev. Lett. **87**, 010404 (2001)
69. M. Schulz, H. Crepaz, F. Schmidt-Kaler, J. Eschner, R. Blatt, J. Mod. Opt. **54**, 1619 (2007)
70. N.G. Parker, N.P. Proukakis, M. Leadbeater, C.S. Adams, Phys. Rev. Lett. **90**, 220401 (2003)
71. N.G. Parker, N.P. Proukakis, C.S. Adams, Phys. Rev. A **81**, 033606 (2010)
72. N.P. Proukakis, N.G. Parker, C.F. Barenghi, C.S. Adams, Phys. Rev. Lett. **93**, 130408 (2004)
73. C.K. Law, C.M. Chan, P.T. Leung, M.-C. Chu, Phys. Rev. Lett. **85**, 1598 (2000)
74. R.R. Sakhel, A.R. Sakhel, H.B. Ghassib, Phys. Rev. A **84**, 033634 (2011)
75. R.R. Sakhel, A.R. Sakhel, H.B. Ghassib, J. Low. Temp. Phys. **173**, 177 (2013)
76. P. Muruganandam, S.K. Adhikari, Comput. Phys. Commun. **180**, 1888 (2009)
77. D. Vudragović, I. Vidanović, A. Balaž, P. Muruganandam, S.K. Adhikari, Comput. Phys. Commun. **183**, 2021 (2012)
78. J. Ruostekoski, B. Kneer, W.P. Schleich, G. Rempe, Phys. Rev. A **63**, 043613 (2001)
79. K. Bongs, S. Burger, G. Birkl, K. Sengstock, W. Ertmer, K. Rzążewski, A. Sanpera, M. Lewenstein, Phys. Rev. Lett. **83**, 3577 (1999)
80. Yan Deng, Wenhua Hai, Gengbiao Lu, Shiguang Rong, J. Phys. B **45**, 135301 (2012)
81. D. Shovan, M.J. Erich, Phys. Rev. A **91**, 013601 (2015)
82. F. Dalfovo, S. Giorgini, L.P. Pitaevskii, S. Stringari, Rev. Mod. Phys. **71**, 463 (1999)
83. C.J. Pethick, H. Smith, *Bose-Einstein Condensation in Dilute Gases* (Cambridge University Press, Cambridge, 2002)
84. P.B. Blakie, A.S. Bradley, M.J. Davis, R.J. Ballagh, C.W. Gardiner, Adv. Phys. **57**, 363 (2008)
85. E.A. Donley, N.R. Claussen, S.L. Cornish, J.L. Roberts, E.A. Cornell, C.E. Wieman, Nature **412**, 295 (2001)
86. J.L. Mateos, J.V. José, Physica A **257**, 434 (1998)
87. O.E. Rössler, Phys. Lett. A **A57**, 397 (1976)
88. G.F.V. Amaral, C. Letellier, L.A. Aguirre, Chaos **16**, 013115 (2006)
89. K. Sasaki, N. Suzuki, H. Saito, Phys. Rev. Lett. **104**, 150404 (2010)
90. F. Schreck, L. Khaykovich, K.L. Corwin, G. Ferrari, T. Bourdel, J. Cubizolles, C. Salomon, Phys. Rev. Lett. **87**, 080403 (2001)
91. O.E. Alon, A.I. Streltsov, L.S. Cederbaum, **77**, 033613 (2008)
92. J. Klaers, J. Schmitt, F. Verwinger, M. Weitz, Nature **468**, 545 (2010)